University of South Florida
Scholar Commons

Graduate Theses and Dissertations

Graduate School

6-24-2016

Inquiry of Lipid Membranes Interacting with Functional Peptides and Polyphenol Drug Molecules

Chian Sing Ho
University of South Florida, cho2@mail.usf.edu

Follow this and additional works at: http://scholarcommons.usf.edu/etd

Part of the Biophysics Commons, and the Physics Commons

Inquiry of Lipid Membranes Interacting with

Functional Peptides and Polyphenol Drug Molecules

by

Chian Sing Ho

A thesis submitted in partial fulfillment
of the requirements for the degree of
Master of Science in Physics
Department of Physics
College of Arts & Sciences
University of South Florida

Major Professor, Jianjun Pan, Ph.D.
Sagar Pandit, Ph.D.
W. Garrett Matthews, Ph.D.

Date of Approval:
June 23, 2016

Keywords: miscibility transition temperature, critical fluctuation, giant unilamellar vesicle, membrane budding, fluorescence mode.

ACKNOWLEDGMENTS

TABLE OF CONTENTS

LIST OF TABLES

LIST OF FIGURES

ACRONYMS

AFM	atomic force microscopy
BF	bright-field
Chol	cholesterol
DMSO	dimethyl sulfoxide
DOPC	1, 2-dioleoyl-sn-glycero-3-phosphocholine
DSC	differential scanning calorimetry
ESCRT	endosomal sorting complex required for transport
ESM	egg-sphingomyelin
FTIR	fourier transform infrared
GUV	giant unilamellar vesicle
HD	huntington's disease
HID	high-intensity discharge
htt	huntingtin
ITO	indium-tin-oxide
L_d	liquid disordered
L_o	liquid ordered
M2TM	M2-transmembrane
Ph	phase contrast
polyQ	polyglutamine
POPC	1-palmitoyl-2-oleoyl-*sn*-glycero-3-phosphatidylcholine
QNM	quantitative nanomechanics
rhodamine-DPPE	1, 2-dipalmitoyl-*sn*-glycero-3-phosphoethanolamine dye

SLB   single lipid bilayer

T_m miscibility transition temperature

ABSTRACT

Cellular membranes are important targets for many membrane-active peptides and drug compounds. Here we are interested in deciphering how lipid membranes are perturbed by several membrane-active molecules, including the transmembrane domain of the influenza M2 protein (M2TM), aggregates formed by a synthetic polyglutamine peptide, and three polyphenol compounds (i.e., tamoxifen, genistein, and verapamil). We employ phase-separated ternary lipid model membranes in the form of giant unilamellar vesicles (GUVs) to simulate raft-like structures that have been proposed to govern many important processes in plasma membranes (e.g., intracellular singling and trafficking). Specifically, we use fluorescent microscopy to interrogate how those membrane additives modulate the phase behavior of free-standing GUVs, as well as the miscibility transition temperature (T_m). We find that M2TM increases T_m and causes vesicle budding; polyglutamine aggregates disrupt lipid membranes; and the three polyphenol compounds exert disparate effects on GUV T_m.

CHAPTER ONE:

INTRODUCTION

1.1: Historical development of cell membrane theory and model

In ancient kingdoms, walls bordering the entire kingdom are vital to its survivability. The defensive walls act as a separation between the chaos outside and the order inside, as well as screening what passes through those walls via gates. Not only that, some kingdoms even had inner walls that separate the *royalty* from the lower class social strata. Ingenuity of humans in history to create kingdoms with walls has long been designed by nature. Humans within themselves carries analogous blueprint for kingdom formation known as cells. Cell membranes are akin to walls surrounding kingdoms.

Since the invention of microscope by Zacharias Janssen, cell membrane theory made its debut through observation of plant's cell wall by Anthony Leeuwenhoek in the 17th century. It took about two centuries later for scientists like Moritz Traube and Heinrich Quincke to formulate cell theory for animal cells. In short, Quincke postulated that cell membranes are made of a layer of fat that is semipermeable [1]. Semipermeable membranes allow the passing of solvent but not solute molecules. A century later, Hugo Fricke added to this understanding by measuring cell membrane thickness to be 3.3 nm [2]. He mistakenly interpreted cell thickness data to be composed of only a single molecular lipid layer. Fast forward a decade later, the first

lipid bilayer model came about from Gorter and Grendel, though it was an inaccurate model

[3]. They attributed membrane permeability to electrostatic repulsion rather than to

hydrophobic tendency found in the core of the membrane. Finally in 1950s, J. David Robertson

with the help of powerful electron microscopy interpreted cell membranes to be of bilayer

nature with hydrophilic headgroups [4].

Going back to late 19th century to early 1970s, a train of distinguished scientists such as

Wilhelm Pfeffer, Ernest Overton, Leonor Michaelis, Seymour Singer and Garth Nicolson to name

a few, helped in constructing what we now have as the fluid mosaic model of cell membranes.

This model shows embedded protein structure within the heterogeneous lipid bilayer

membranes (Figure 1).
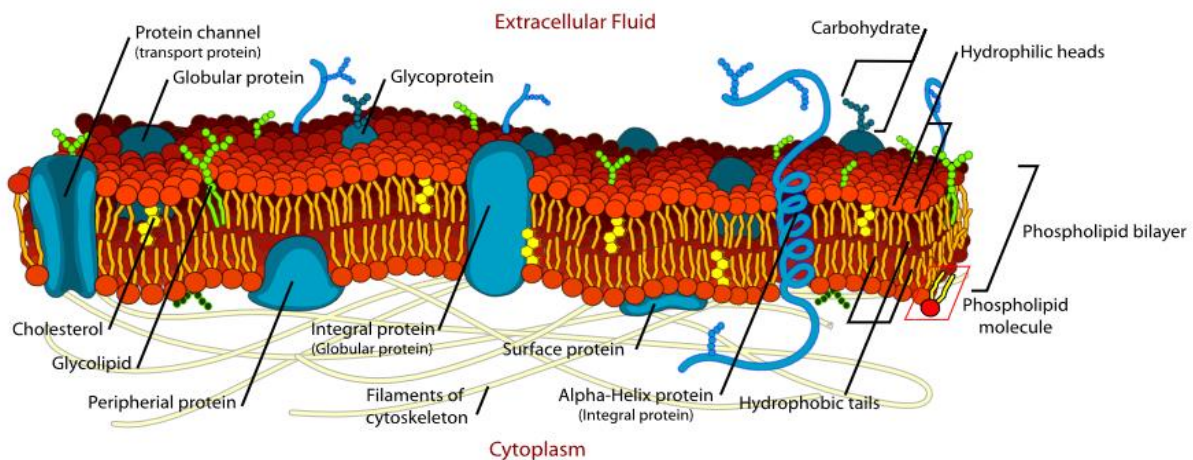
Figure 1: Fluid Mosaic Model of cell membranes developed by Singer and Nicolson in 1972. The
model shows opposing headgroups away from the hydrophobic center. There are also proteins
embedded partially/fully within the membrane. These proteins are free to move around its
surrounding liquid bilayer. Image source:
https://commons.wikimedia.org/wiki/File%3ACell_membrane_detailed_diagram_en.svg

1.2: Outline of the thesis

This thesis work focuses on the interaction study between various peptide/polyphenol molecules with lipid membranes in the form of giant unilamellar vesicles (GUVs). Specifically, addition of peptides or polyphenol molecules alters intrinsic properties of lipid membranes such as miscibility transition temperature (T_m) and membrane curvature. There are four major parts that make up this masters thesis. First, GUVs of various lipid compositions were concocted to study how lipid compositions modulate GUV phase separation. Cell membranes contain raft-like structures that are more rigid compare to its "lax" surrounding. In model membranes, liquid-ordered (L_o) phase is analogous to lipid rafts while liquid-disordered (L_d) phase is analogous to the "lax" surrounding [5]. GUVs with L_o and L_d phase separation have been suggested as reasonable models to represent heterogeneous organiziton in cell plasma membranes. Part two covers the transmembrane domain of influenza M2 protein (M2TM) addition to GUVs. Part three discusses the consequences of adding aggregates formed by a syntemtic polyglutamine (polyQ) peptide to GUVs. This work conlcudes with studying the effect of polyphenol molecules on the miscibility transition temperatire T_m of ternary GUVs. (T_m studies were also performed for pure GUVs and M2TM-premixed GUVs.) In T_m study, temperature was monitored when phase coexisting GUVs become homogeneous. Fluroescent images of dye-doped GUVs were taken to observe membrane deformation.

1.3: Important instruments

Optical microscope was heavily utilized in this work. To show phase separation in L_o-L_d phase coexisting GUVs, two modes of microscope imaging were used, i.e., bright field and epifluorescence. In both modes, L_o phase corresponds to the dark region on GUVs and the L_d phase corresponds to the bright region (i.e., the dye molecules used preferentially partition into the disordered L_d phase). GUVs with ~30 µm diameter were used. GUVs were produced from lipid mixtures using the electroformation process described by Angelova [6]. A temperature probe (Type T) was placed inside an isolated custom-built copper chamber to measure GUV miscibility transition temperature T_m. For comparison, atomic force microscopy data were also presented.

1.4: Reasons of the studies

There are many reasons why the studies in this thesis are useful. The influenza A virus for example depends on M2 peptide for virus invasion, replication and egress. It is known that the endosomal sorting complex required for transport (ESCRT) is not responsible for influenza A virus budding and scission. Hence a better understanding on how M2 peptide hijacks host cell membranes is crucial [7]. It is also important to better understand how polyQ aggregates disrupt lipid membranes. Pathogenic expansion of the CAG repeat in the gene encoding huntingtin (*htt*) protein leads to the formation of polyQ mediated aggregates that are probably responsible for the progressive neuronal Huntington's disease (HD) in humans [8]. Polyphenol molecules like tamoxifen and genistein are similar to each other functionally when it comes to prevention of breast cancer. Tamoxifen has been widely used as an anticancer drug because of

its ability to compete with endogenous estrogen-receptor binding sites [9]. Verapamil is a calcium channel blocker that treats hypertension, angina, and cardiac dysrhythmia. Thus studies of these polyphenol molecules will enlighten us on molecular interactions with lipid membranes so that we could improve on current available drugs.

CHAPTER TWO:

INSTRUMENTATIONS AND METHODOLOGY

2.1: Introduction

This thesis work began around August of 2014 in trying to study phase separation of

ternary GUVs. A year into working in the lab, Dr. Pan came to acquire a state of the art atomic

force microscopy (AFM). This instrument will be introduced briefly at the end of this chapter as

many of AFM works has been complimentary to this thesis work. This chapter will discuss

instrumentations such as the light microscopy and electroformation method, central to this

work.

2.2: Electroformation methods and instrumentation

This section will cover lipids used and instrumentation for GUV synthesis. The process

for synthesizing GUVs is called electroformation. In this process, two electrodes with deposited

lipids are surrounded in aqueous solution. The electrodes will be attached to a function

generator to generate AC voltage. This alternating voltage will excite both electrodes at a

certain frequency, causing the lipids deposited on the electrodes to swell and aggregate

according to hydrophobicity. All of the chemicals, lipids, and drug molecules are purchased

from Avanti Polar Lipids, Sigma Aldrich, and Fisher Scientific. PolyQ peptide (KK-Q$_{35}$-KK) and

M2TM peptide (residues 22-46 of M2 protein, SSDPLVVAASIMGILHLILWILDRL) were either

synthesized by our collaborator, Dr. Jianfeng Cai's group in the Department of Chemistry (USF), or by the Peptide Synthesis Center at USF (http://chemistry.usf.edu/research/peptide/). The two peptides are both prepared by solid phase synthesis method, HPLC purification, and lyophilization. Lipids, including 1-palmitoyl-2-oleoyl-*sn*-glycero-3-phosphocholine (POPC), 1, 2-dioleoyl-*sn*-glycero-3-phosphocholine (DOPC), egg-sphingomyelin (ESM), cholesterol (Chol), and the dye molecule 1, 2-dipalmitoyl-*sn*-glycero-3-phosphoethanolamine (rhodamine-DPPE) were prepared in chloroform or chloroform/methanol 3:1 v/v as stock solutions and stored at -80°C. Similarly, stock solutions of M2TM, tamoxifen, genistein, and verapamil are prepared and stored at -80°C. For polyQ, aggregates are formed by dissolving the peptide in 10 mM HEPES pH 7.4 buffer and stored at 4°C.

2.2.1: Lipids

Ternary mixtures of DOPC, ESM, and cholesterol were used in preparing GUVs through electroformation method described by Angelova et al [6]. 0.2mol% rhodamine-DPPE dye was added to lipid mixtures for fluorescence imaging. Electroformation is performed at high temperature (60°C). GUVs prepared have lipid ratios ranging from 1:1 to 3:1 (DOPC:SM mol/mol) with 0-50 mol% Chol. (All lipid mixtures were prepared in mole ratio, fraction, or percentage.) Within this lipid ratio region, vesicles have been shown to contain both L_o and L_d phases as well as exhibiting interesting critical-like fluctuations when temperature is elevated [10].

2.2.2: Pre-Electroformation

Proper amounts of lipid stock solutions were mixed into a 10ml glass test tube. This mixture was sonicated and vortex briefly to ensure lipid homogeneity. Instead of electrode, Indium-Tin-Oxide (ITO) glass slides were used as conductor. ITO slides are only coated on one side. The homogenous lipid mixture was smeared onto heated ITO slides (~60°C) and vacuumed for 1 hour to remove any excess organic solvents. ITO slides were sandwiched with O-rings like in Figure 2. The aqueous solution used here was 100 mM sucrose and 10 mM HEPES @ pH7.0. Figure 3 shows instruments used.
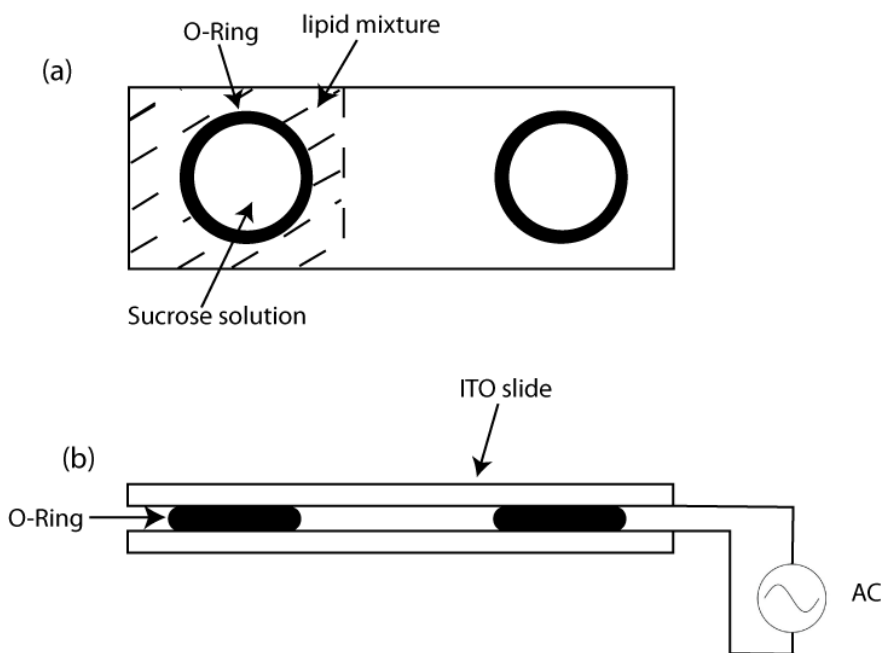
Figure 2: Electroformation setup using ITO-glass slides, O-rings, and AC power supply. (a) Ternary lipid mixture smeared on the top conductive side of 2 cleaned and heated ITO slides. O-ring acted as a container for the sucrose solution needed for GUV formation. (b) ITO slides sandwiched as illustrated and AC voltage (2 V) applied with temperature at 60 ± 5°C. Heating element is not shown here.

Figure 3: a) *Left:* Fisher Scientific™ Digital Vortex Mixer *Right:* Fisher Scientific™ MH Series Mechanical Ultrasonic Cleaners. b) *Left:* Benchmark Scientific H3760-HS-E *Right:* Across International VO-16020m *Bottom:* Robinair 2-Stage Vacuum Pump 15500.

2.2.3: GUV synthesis

The slide sandwiches shown in Figure 2 were slotted inside an in-house built aluminum heating block. Electroformation setup is shown in Figure 4. Alligator clips (insulator-coated outside, red color) were clipped on to the ITO slides and was used to deliver AC voltage produced by the function generator. Aluminum heating block was heated by dry bath incubator controlled by Digi-Sense Type-T temperature controller. Function generator was set to 2V @ 10Hz for 2 hours and temperature at 60°C. After 2 hours, AC voltage was turned off and temperature was slowly cooled down to room temperature.
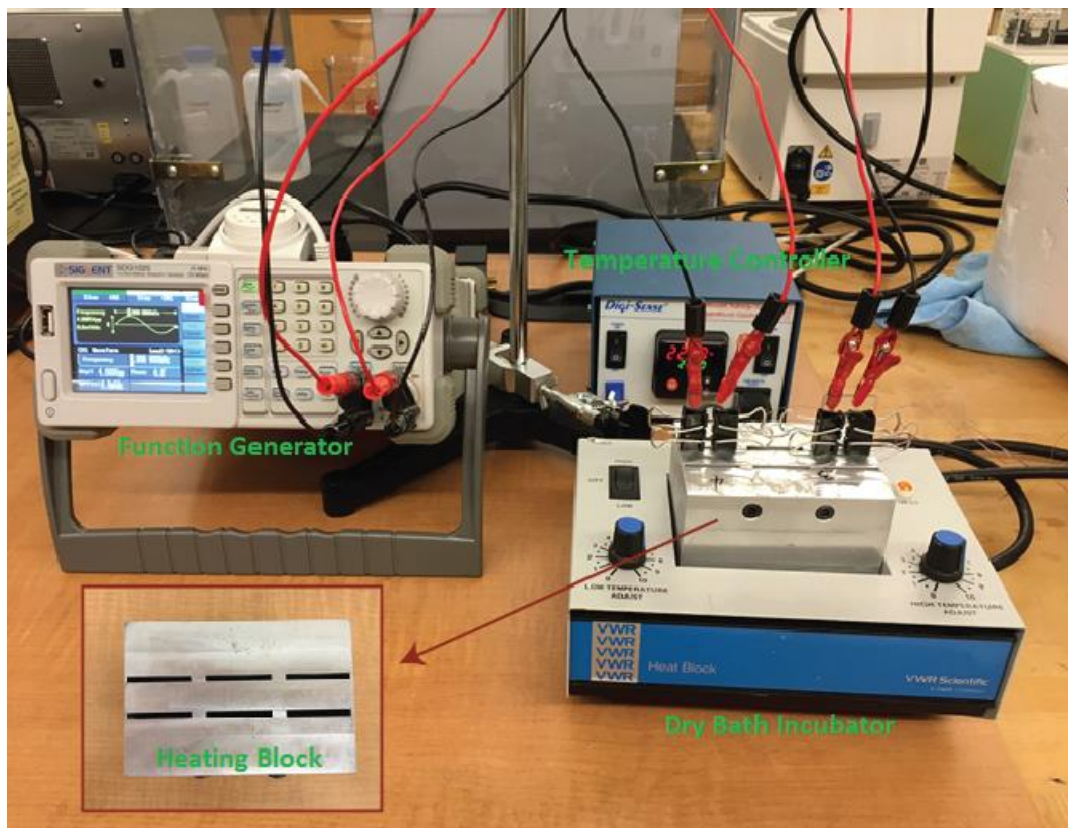
Figure 4: Setup of electroformation method. Function generator operates at 2 V AC voltage, 10 Hz, and a sine waveform for 2 hours. Temperature was set to 60°C for 2 hours and then slowly cooled down to room temperature. Instruments include Siglent SDG1025 Function Generator, Digi-Sense T-Type Temperature Controller, and VWR 13259-005 Dry Bath Incubator.

2.2.4: Post-Electroformation

After cooling down to room temperature, GUVs were harvested into 100 mM fresh glucose and 10mM HEPES @ pH 7.0 solution. GUVs were viewed within the day of preparation itself, but not at least 30 minutes after harvesting. Visit http://faculty.cas.usf.edu/pan/videos.html for a complete video presentation of the electroformation method.

2.3: Light Microscopy

Optical microscope is an analytical tool that enables a researcher to view specimen up to 1000x its original size. Meaningful microscope magnification can go up to 1500x. The downside to high magnification is low intensity. The principle of a bright filed optical microscope is fairly simple. Light source emits light rays that are focused by a condenser that converges on the specimen. Light rays that illuminate the specimen will continue to diverge past the specimen and be magnified by an objective lens. The image produced by the objective lens will be inverted. Another lens known as the ocular/eyepiece lens will further magnify the image into our eyes and correct the inverted image, resulting in an upright final image. Image magnification can be calculated by multiplying the objective lens and the ocular lens. Figure 5 shows a diagram of the light path in a basic microscope.
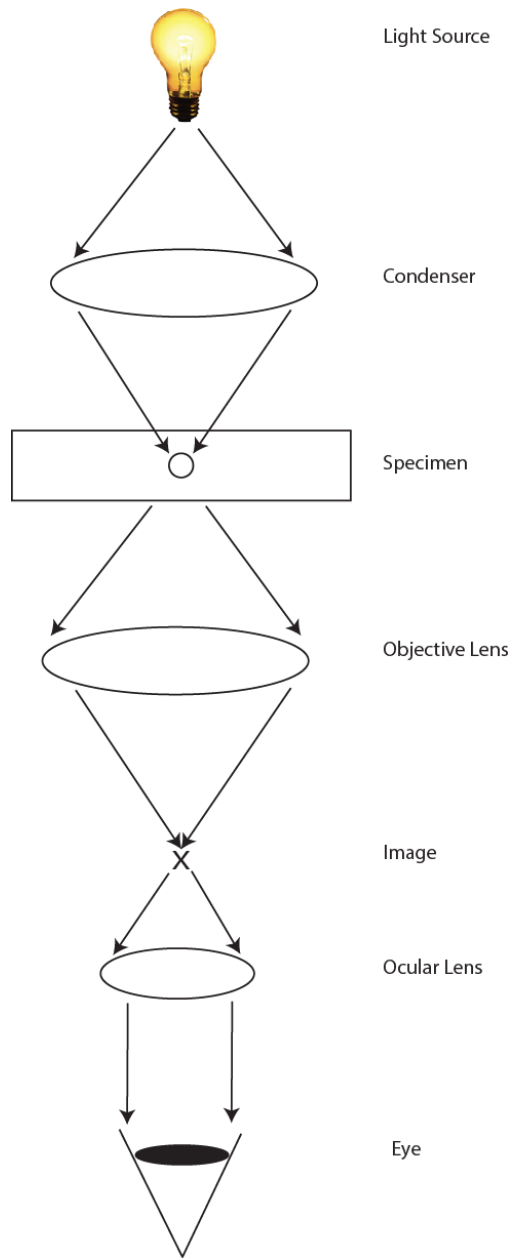
Figure 5: Basic light path of an optical microscope. Light rays from the light source pass through the condenser and converge onto the specimen. The light that illuminates the specimen will reach the objective lens and form a magnified, inverted image. The image is further magnified by the ocular lens that falls into eyes. Magnification is determined by multiplying objective lens and ocular lens.

Nikon ECLIPSE T*i*-U inverted microscope was heavily employed in this thesis work. Besides

bright filed light microscopy, fluorescent microscopy was also utilized. Fluorescent microscopy

has a different light source compared to bright filed light microscopy, a metal-halide lamp. This

light source actually emits from the bottom of the specimen instead from the top in light

microscopy mode. Main components of this inverted microscope will be explained below

(Figure 6).
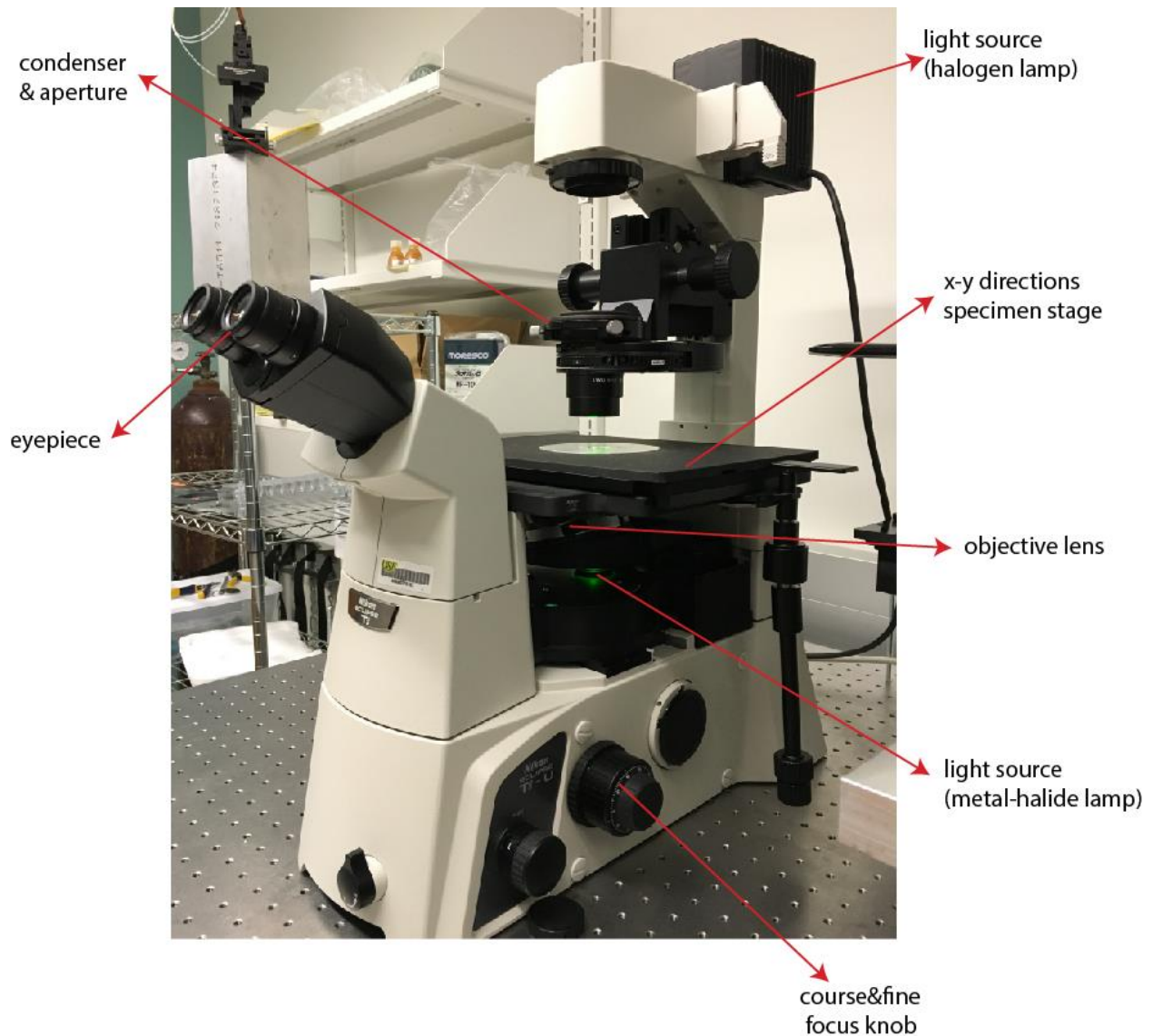
Figure 6: Nikon ECLIPSE T*i*-U inverted microscope showing important components. Andor iXon
Ultra 897 EMCCD is attached on the other side (not visible).

2.3.1: Light sources

There are two types of light sources built into this microscope: halogen lamp and metal-halide lamp. The halogen lamp runs on TI-PS 100W power supply for 100-240V. This halogenic light is used for viewing phase contrast (Ph) and bright-field (BF) of a specimen. In this mode, a dense area on a specimen will absorb the halogenic light and make that region dark, while the less dense areas will transmit halogenic light and appear bright. The metal-halide lamp runs on Prior L200US 250W power supply for 110-240V. This lamp is a type of high-intensity discharge (HID) gas discharge lamp and is used for viewing fluoro-luminescence specimen, known as fluorescent microscopy. A specimen needs to be dyed by fluorophores prior to using this imaging mode. When light hits specimen, areas on the specimen that contain fluorophores will be excited by the light by absorbing photons, and then re-emitting light with a different wavelength photons. Figure 7 shows power supplies for both imaging modes.
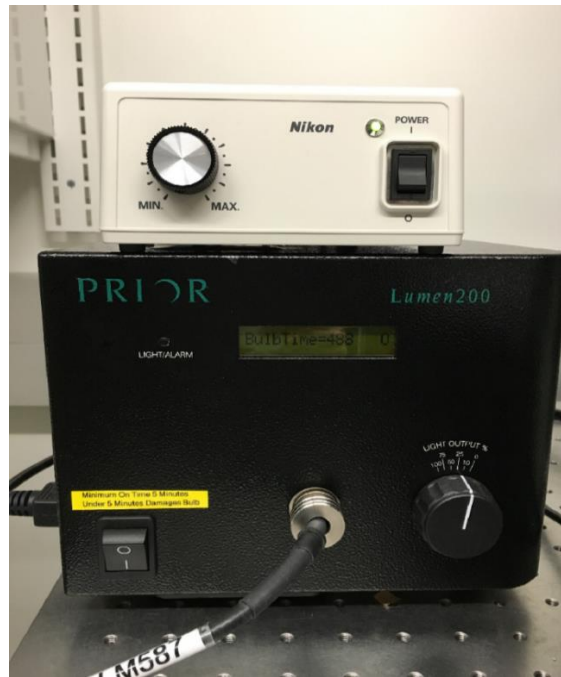
Figure 7: Top shows TI-PS 100W power supply for 100-240V used in bright-field mode. Bottom shows Prior L200US 250W power supply for 110-240V used in fluorescent mode.

2.3.2: Objective lens

Objective lens is key to magnifying specimens. The objective lens collects light rays from illuminated specimen and projects an inverted image. We have objective lenses with different magnifications (4-100x). 4-10x are low powered objectives. These objectives are good for viewing tissues and selecting regions of interest on a specimen. For high powered objectives, lenses range from 40-100x. These objectives are used to view cells and submicron specimen. As magnification increases, resolution length also increases, causing the image to have low intensity. Because of this, many objectives use fluid-based objectives such as oil-, water-, glycerol-immersion. The fluid's large index of refraction helps to gather light rays into the objective lens, hence increases the intensity. Air-immersion long working distance CFI super fluor ELWD 60x was used for most of our GUV imaging.

2.3.3: Condenser and aperture

Condenser allows light rays to be focused on the specimen. In Nikon Eclipse T*i*-U, there are three imaging modes built into the microscope; BF, Ph, and external phase contrast. Imaging modes are interchangeable by rotating turret that carries various optical elements. Aperture diaphragm on the other hand, adjusts the size of field of view. The calibration of condenser and aperture diaphragm are only important for BF and Ph imaging modes. Most of this work was done in fluorescent mode.

2.3.4: Specimen stage and preparation

A specimen can be moved in x and y directions when mounted on the stage. Custom sample chamber was designed to accommodate small working distance of the objective lens. Sample preparation was done by further diluting harvested GUVs with 100 mM glucose and 10 mM HEPES @ pH7.0 solution and then pipetted to a silicone gel well covered with cover slip on a glass slide. Cover slip will orient closest to the objective lens. GUVs images were obtained with Nikon Eclipse T*i*-U equipped with Andor iXon Ultra 897 EMCCD camera. Coupled with highly complementary microscope software (NIS-Element), we were able to record GUV videos and capture images. 60x objective and 500 ms exposure time were used to take images and record videos (1 sec interval/frame). GUVs with fully L_d phase, L_o-L_d coexisting phases, and critical-like fluctuations were observed under fluorescent condition. L_d phase appears bright due to segregation of rhodamine-DPPE dye in that phase.

16

2.3.5: Focusing knob

As the specimen stage allows x and y directions movements, focusing knob allows z direction movement of the objective lens. Focusing knob displaces the height of the objective lens relative to the specimen stage. There are two focusing sensitivity, coarse and fine focusing. Focusing is crucial to bring objective lens to its working distance in order for lens to function correctly. Since the sample cover slip will be closest to the objective lens, there will be "bead-like" artifacts coming into focus first from coarse focusing. Upon seeing those artifacts, fine focusing was used to locate GUVs. Majority of GUVs were sunken down at the bottom of the sample chamber as sample was allowed to sit for 30 minutes prior to imaging.

2.3.6: Temperature-controlled chamber for temperature-sensitive environment

Since studies of GUV phase miscibility transition temperature T_m require stable environmental temperature surrounding the sample, a temperature-controlled chamber was machined out of copper to allow for both BF and fluorescent microscopy. The chamber is heated by a Thermo Scientific Haake ARCTIC A25 coupled with an AC 150 Immersion Bath Circulator. A water canal was machined inside the chamber and is connected to the bath circulator. A temperature probe (Type T) was used to measure the temperature of the sample. The probe was directly inserted into the sample solution via a small hole drilled through a plastic microscope slide. Temperature was read by Digi-Sense Temperature Controller (see Figure 4). Figure 8 shows the physical placing of chamber on the specimen stage. This in-house observation chamber was able to acquire down to 0.1°C precision.

Using this observation chamber, T_m study was performed for M2TM, tamoxifen, genistein, verapamil and pure lipid mixtures. Polyphenol molecules and M2TM (by mol%) were added to lipid mixtures prior to electroformation to obtain appropriate GUVs for experiments. To avoid T_m hysteresis (i.e., T_m could be different depending on heating or cooling GUVs), all temperature ramping experiments were done by cooling from high to low temperatures.
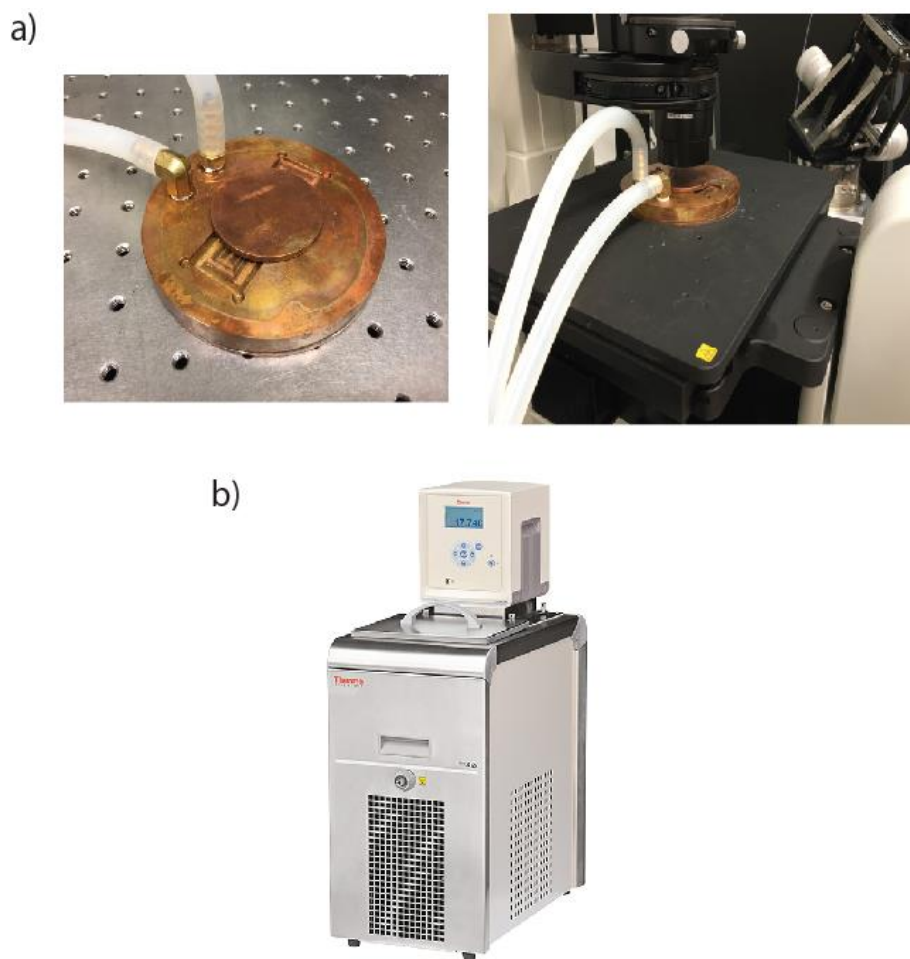
Figure 8: a) *Left:* Copper temperature-controlled chamber with a removable top. Water tubes are connected to bath circulator. *Right:* Placement of temperature-controlled chamber on top of the specimen on the stage. The top can be removed to allow for BF imaging. b) Thermo Scientific Haake ARCTIC A25 coupled with AC 150 Immersion Bath Circulator used for heating and cooling. Ultrapure water (18.2 ΩM-cm) was used as circulatory heating fluid.

2.4: Atomic Force Microscopy

Atomic force microscope (AFM) is a powerful analytical tool because it can acquire nanoscale three-dimensional specimen topography as well as material properties (e.g., Young's modulus). The first AFM was invented by Binnig et al. in 1986 [11]. AFM scans sample surface through a probe known as the "*tip*". This *tip* is attached to a cantilever arm which has a deflective surface on the opposite side of the *tip,* on the cantilever arm. The deflective surface acts to deflect the laser beam focused on the top of the *tip* and the deflected beam is detector by a photodiode. As the *tip* scans across, height difference on the specimen surface will move the *tip* in the z-direction*,* hence moving the laser detected by the photodiode and result in a topographical map. Since the *tip* will be nanometers away from the surface, there are few forces that deflects the cantilever arm. These forces are repulsive force, electrostatic attractive force, and capillary force (in fluid). Ever since the invention of AFM contact mode, more imaging modes have been introduced. There is now non-contact mode, tapping mode, PeakForce quantitative nanomechanics (QNM) mode, and many more. To complement GUVs studies, we also used a fluid-compatible Multimode 8 AFM from Bruker to measure planar lipid bilayer topography in response to foreign molecules [12, 13]. Figure 9 shows an example of height images for a ternary lipid system exhibiting large and small phase separation near the critical point [14].
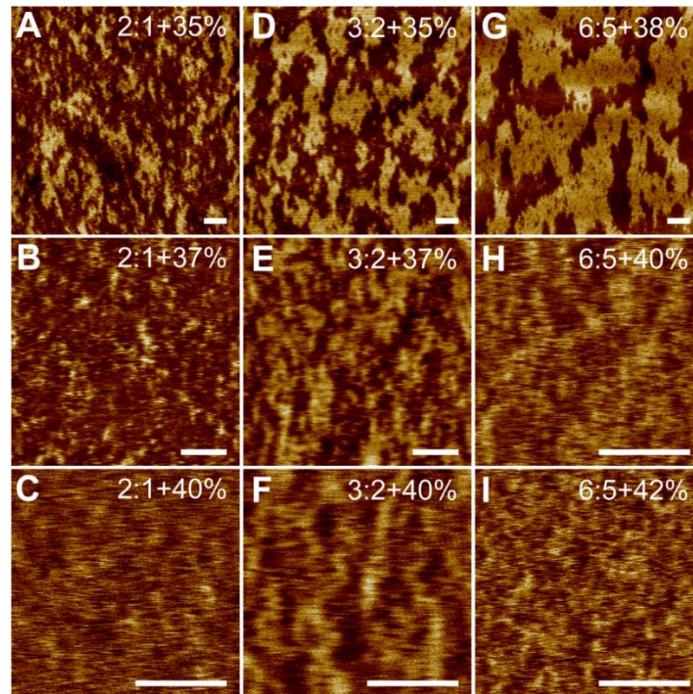
Figure 9: Height images of a ternary lipid system (DOPC/ESM/Chol) taken from *"Macroscopic and Nanoscopic Heterogeneous Structures in a Three-Component Lipid Bilayer Mixtures Determined by Atomic Force Microscopy"* paper [14]. Lipid compositions are indicated by the ratio of DOPC:eSM + cholesterol mole percentage. Scale bars are 200 nm.

CHAPTER THREE:

GIANT UNILAMELLAR VESICLES

3.1: Brief introduction to phospholipid and lipid bilayer

Cellular membranes (e.g., outer plasma membranes and inner membranes enveloping nucleus, mitochondria, Golgi apparatus, and endoplasmic reticulum, etc.) contain many lipid species, including fats, sterols, phospholipids, mono-/bi-/tri-glycerides, sphingolipids, gangliosides, and many more. Despite the diversity of lipid species to choose from, it is well-known that phospholipids are the most abundant lipids that constitute a cell membrane. Phospholipids are generally separated into two regions: polar hydrophilic headgroup and two hydrophobic fatty acid chains aka acyl chains (Figure 10). The hydrophilicity of the headgroup is due to the negatively charged phosphate group. This phosphate group is also connected to a glycerol backbone. On the other hand, the acyl chains are uncharged, therefore do not have an affinity towards aqueous solution like water. Within the acyl chain, there are saturated (single bonds) and unsaturated (double bonds) carbon bonds. The region on membrane where it is made up of saturated acyl chains is generally stiffer than the region with unsaturated chains.
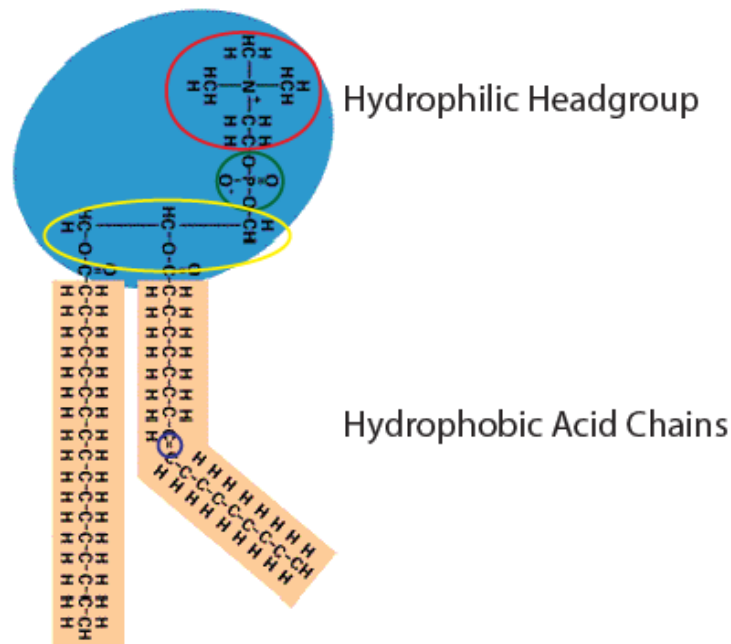
Figure 10: Chemical structure of a phospholipid. Hydrophilic headgroup is composed of choline (red circle), phosphate (green circle), and glycerol (yellow circle). Hydrophobic acid chains can be either saturated (left) chain or unsaturated (right) chain with double bond (blue circle) making a "kink" in the chain. Image source: http://myhome.sunyocc.edu/~weiskirl/lipids_membranes.htm

When lipids self-assemble, the hydrophobic tails will tend to group together (away from water), leaving headgroup exposed to the aqueous solution. This amphipathic behavior of lipids leads to the natural formation of membranes. There are different morphologies for lipid membrane structures, including liposome, bilayer sheet, and micelle, to name a few. In this work, the structure of liposomes best resembles cell membranes and was therefore utilized. Recently, Beltramo et al. developed a free-standing model of lipid membranes [15]. This model allows probing on both sides of the membrane as oppose to the older models mentioned above.

As mentioned in Chapter 1, the function of cell membranes is to keep foreign molecules out and protect important organelles for the cell to operate properly. Cell membranes also function as a "gate" to allow smaller molecules to past through for important cellular processes. It is helpful to determine a reasonable lipid composition for in-vitro model membrane. GUV formation and imaging are explained in Chapter 2. Phase separation is observed in many electroformed GUVs. Also, there is a corresponding correlation between the amount of saturated lipid presenting in GUVs to the surface area of L_o. Lastly, the phase miscibility transition temperature T_m of GUVs composed of 3:2 DOPC/ESM + 32mol% Chol was determined to be 32.7°C.

3.2: Phase separated GUV behavior

GUVs have become a favorable model for many contemporary studies of lipid membranes since early 1970s [5]. It is clear that phase separation was observed in ternary system GUVs. Prior to using DOPC/ESM/Chol mixtures, alternate mixtures containing POPC were investigated (i.e., POPC/brain-sphingomyelin/Chol). It was revealing to find that POPC-containing mixtures posed issue for phase separation study as it is homogenous under fluorescence microscopy. The nano-scale phase separation behavior can only be unveiled by a much more powerful tool, such as AFM. We have conducted an experiment of a four-component lipid bilayer system (DOPC/POPC/brain-sphingomyelin/Chol) with DOPC slowly replacing POPC and confirmed that DOPC induces micro-structure while POPC induces nano-structure [16].

The difference between DOPC and POPC is found in the hydrocarbon chains. POPC contains one unsaturated (C=C double bond) acyl chain and DOPC contains two unsaturated acyl chains. These unsaturated acyl chains are what makes membrane tight packing hard [17]. Sphingolipids (egg-sphingomyelin and brain-sphingomyelin) contain saturated acyl chains that are ideal for order and tight packing. In general, the unsaturated acyl chains like to stay with unsaturated chains, and saturated chains will like to stay with saturated chains. Therefore, DOPC will mix poorly with sphingolipids, while POPC will have better mixing tendency with sphingolipids. This qualitatively explains why large phase separation is observed in DOPC-containing mixtures, but not in POPC-containing mixtures.

During observation, not all GUVs from the same sample display the same phase behavior. Some would have more L_o domain surface area than others, and some would not phase-separate at all. This is due to the compositional heterogeneity that exists during the process of electroformation [18]. On a different note, a group has shown that domain formation can also be photo-activated if GUVs are exposed to light for some time [19]. Finally, T_m of a lipid composition differs as temperature ramping path follows a hysteresis loop [20]. To tackle the first issue, over 30 individual GUVs were recorded that display similar phase behavior at a given temperature to ensure bulk phase behavior of that sample. Next, exposure of GUVs to fluorescent light was limited by only focusing on small area of the glass slide and blocking off the light when not imaging. Temperature ramping pattern has been kept the same for all T_m study (from high to low temperature) to ensure all T_m are on the same side of the hysteresis loop. Another countermeasure that was taken was to make a control sample every time we

24

made a new lipid composition. The control sample acts as a reference point to connect all lipid compositions.

3.3: Lipid compositions

The work of increasing sphingolipid (i.e, ESM) ratio in the lipid mixture of (DOPC/ESM/Chol), shows increase of surface area of tightly packed L_o phase [14]. This L_o phase corresponds to the dark region in Figure 11. Contrary, the loosely packed unsaturated DOPC enriched L_d phase corresponds to the bright region under fluorescent microscopy in Figure 11. The brightness of L_d phase comes from the rhodamine-DPPE dye, which preferentially partitions into the L_d phase.
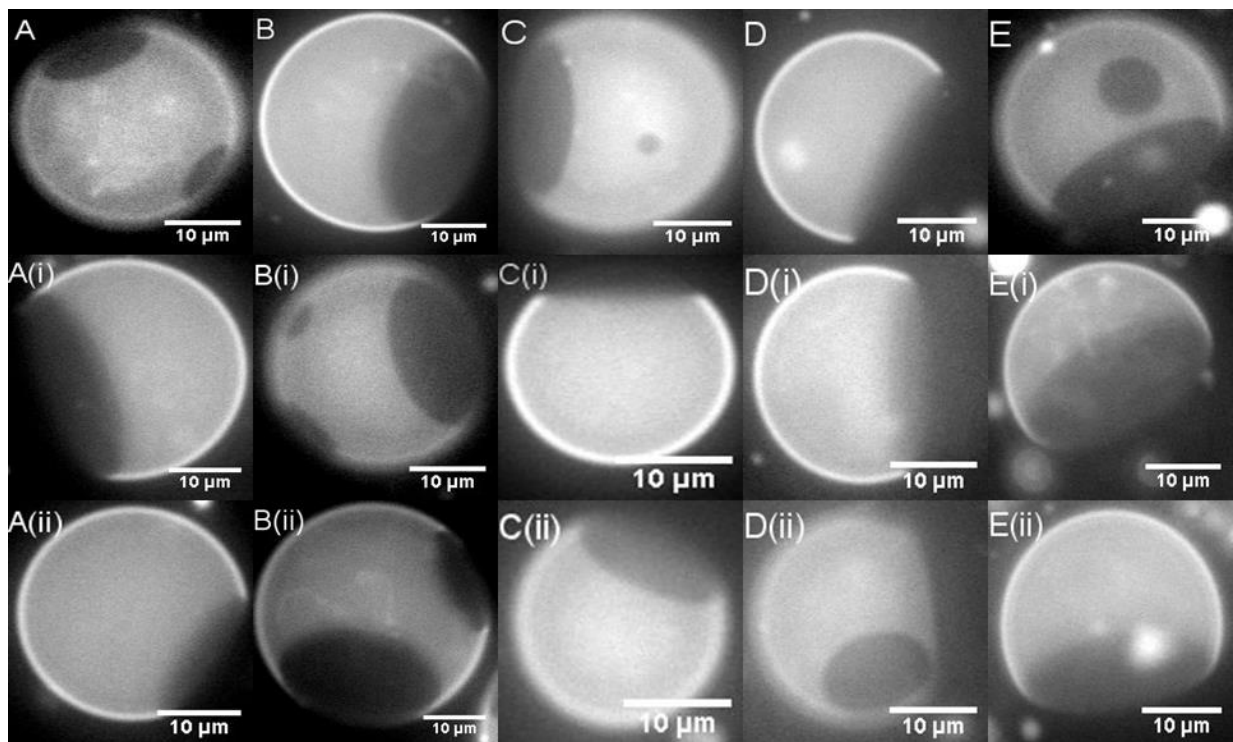
Figure 11: Above shows fluorescence GUVs (@27°C) of various DOPC:ESM ratio +20mol% Chol; (A) 3:1; (B) 2:1;(C) 12:7; (D) 3:2; and (E) 1:1. L_d phase dominates at low ESM content, while L_o phase increased as ESM content increased.

Though the surface area fraction of L_o/L_d phase is not prominent in Figure 11, one can still see

the gradual area fraction increase from 3:1 to 1:1 ratio. L_o surface area fraction drastically

increased as ESM is added past 1:1 ratio, which served as a threshold ratio for L_o phase

domination, shown in Figure 12. GUVs did not become one L_o phase despite fourfold ratio of

ESM to DOPC (Figure 12C). GUV appears to have two kinds of Lo domains; hemispherical

capped and island-like. Images of these GUVs were taken several hours post-electroformation

and at room temperature (27°C). GUV studies in this section were all observed in room

temperature unless stated otherwise. This can mean given enough time for lipids to

agglomerate, a single large L_o domain is more favorable than many L_o domains.
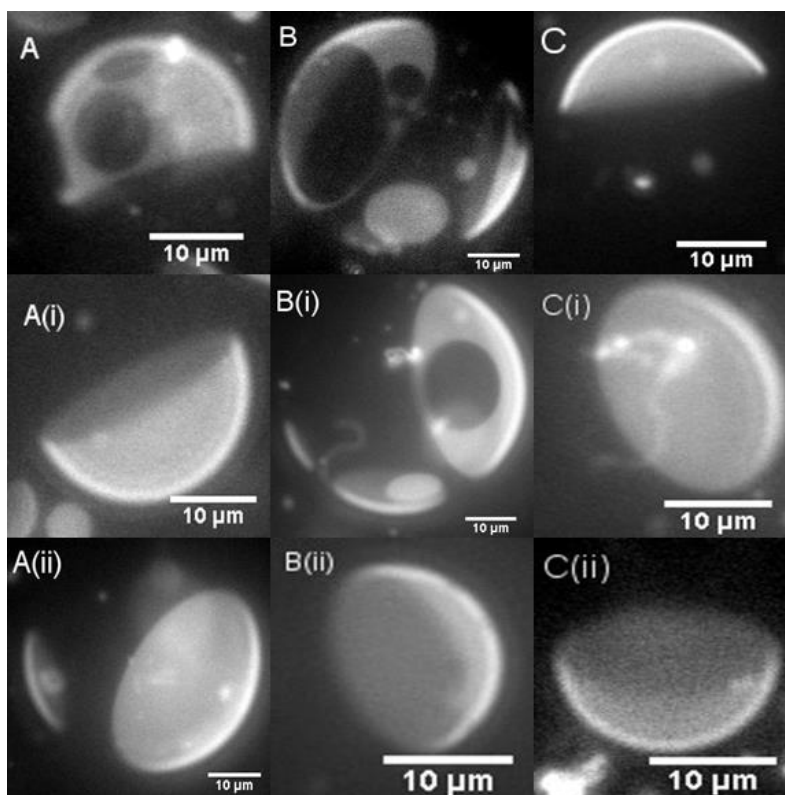
Figure 12: Above shows fluorescence GUVs in ternary lipid mixture of DOPC:ESM+cholesterol in various DOPC to ESM ratio; (A) 1:2; (B) 1:3; and (C) 1:4. Cholesterol concentration was held at 25%. L_o phase dominates at high ESM content.

3.4: Effect of cholesterol on GUVs

The exhausted study of saturated-unsaturated lipid mixtures led to the examination of cholesterol effects in GUVs. GUVs of DOPC/ESM ratios 1:1, 3:2, and 2:1 were examined with various cholesterol %. For 1:1 ratio, 20% Chol seems to produce a hemispherical L_o phase that persists even at 30% Chol (Figure 13B, C). At 38% Chol, the well-defined boundary between L_o and L_d phases deconstruct into coexisting undulation of L_o-L_d (shown in Figure 13E). As Chol content increased to 42%, GUVs developed into a homogenous L_o phase (Figure 13F).
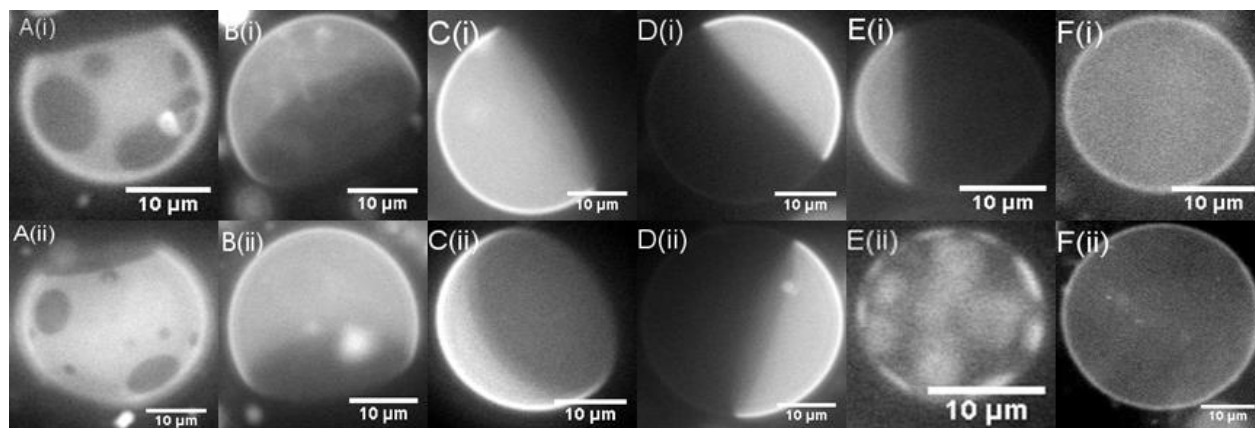
Figure 13: Above shows fluorescence GUVs in ternary lipid mixture of (1:1) DOPC:ESM in various Chol concentration; (A) 10%; (B) 20%; (C) 30%; (D) 35%; (E) 38%; (some GUVs may display compositional deviation); and (F) 42%-*one L_o phase*. Images of GUVs were taken at room temperature (27°C).

Evidently, addition of Chol increases L_o surface area which is similar to addition of ESM. For 3:2 ratio, critical fluctuation occurs at 35% Chol (Figure 14E) while homogenous L_o phase occurs at 38% Chol (Figure 14F).
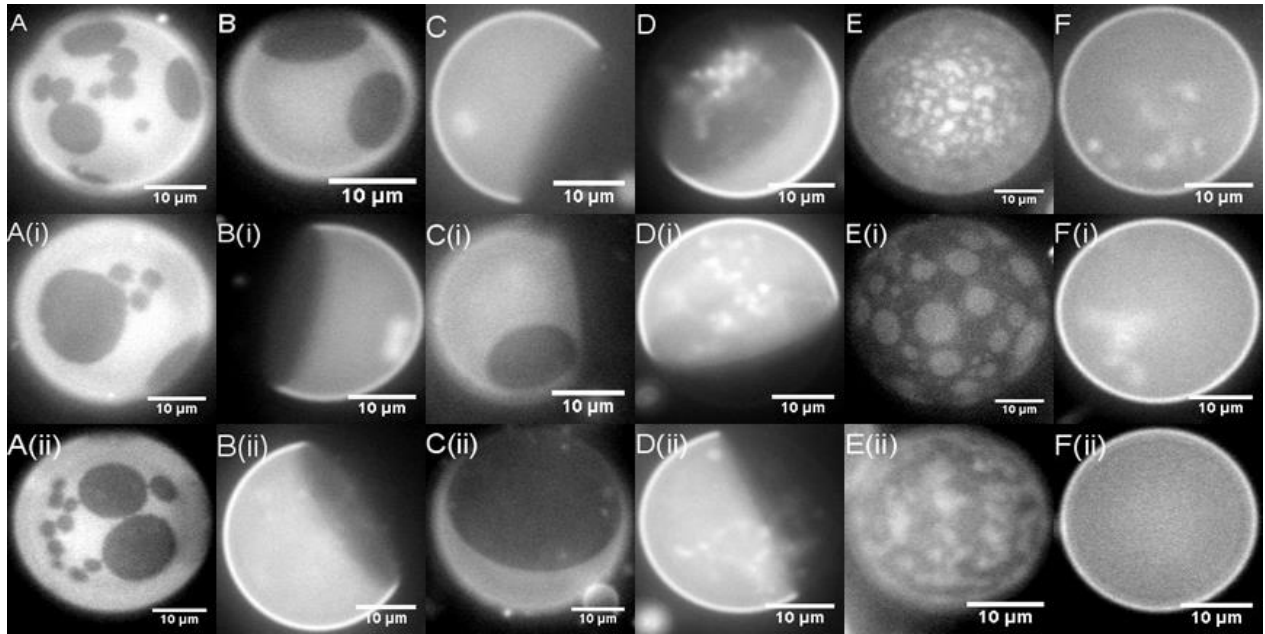
Figure 14: Above shows fluorescence GUVs in ternary lipid mixture of DOPC/ESM 3:2 in various Chol concentration; (A) 5%; (B) 10%; (C) 20%; (D) 30%; (E) 35%-*critical fluctuations*; and (F) 38%-*one L_o phase*. Images of GUVs were taken at room temperature (27°C).

The trend follows as critical fluctuations for 2:1 ratio decreased down to 33% Chol (Figure 15D) and homogenous L_o phase at 35% Chol (Figure 15E). A summary of various lipid ratios experiencing critical fluctuations is shown in Figure 16. These critical fluctuations are in submicron scale and have irregular shapes. The irregular shapes arise from the high maneuverability of the L_o-L_d undulation compared to low maneuverability of distinct phase separation.
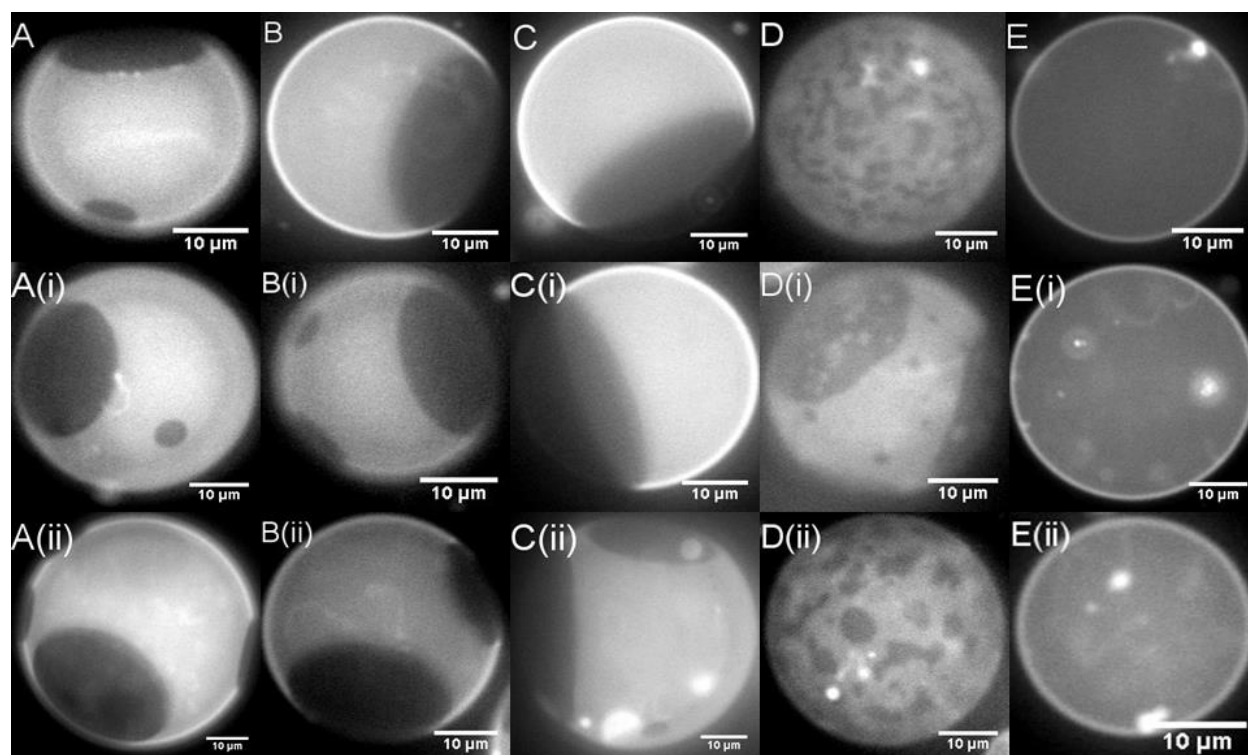
Figure 15: Above shows fluorescence GUVs in ternary lipid mixture of DOPC/ESM 2:1 in various Chol concentration; (A) 10%; (B) 20%; (C) 30%; (D) 33%-*critical fluctuations*; and (E) 35%-*one L_o phase*. Images of GUVs were taken at room temperature (27°C).
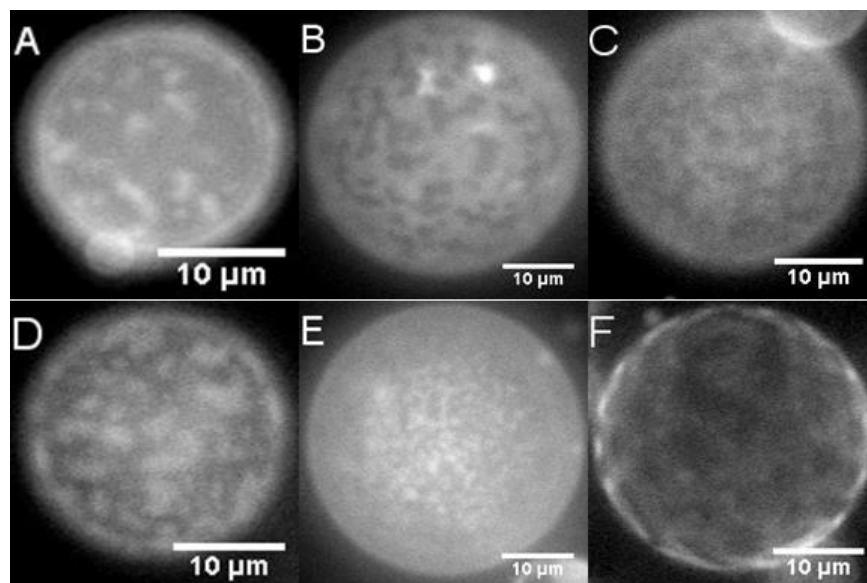
Figure 16: The fluorescence GUVs showing critical fluctuations at different ternary lipid mixtures of DOPC:SM + %Chol at room temperature (27°C); (A) 3:1+30%; (B) 2:1+33%; (C) 12:7+36%; (D) 3:2+35%; (E) 6:5+37%; (F) 1:1+38%.

The finding in Figure 14 shows that addition of cholesterol enhances the surface area of L_o

domain. Since the majority of cholesterol is associated with the Lo phase, it seems that the rigid

ring structure of cholesterol is more compatible with saturated sphingolipids, resulting in

decreased mobility of the acyl chains of sphingolipids [21] (Figure 17). It has been proposed

that the small polar head of cholesterol is what allows it to orient itself close to the membrane

surface and next to the phospholipid headgroups [22]. Cholesterol-saturated lipid interaction

has also been attributed to strong hydrogen bond between those two [23].
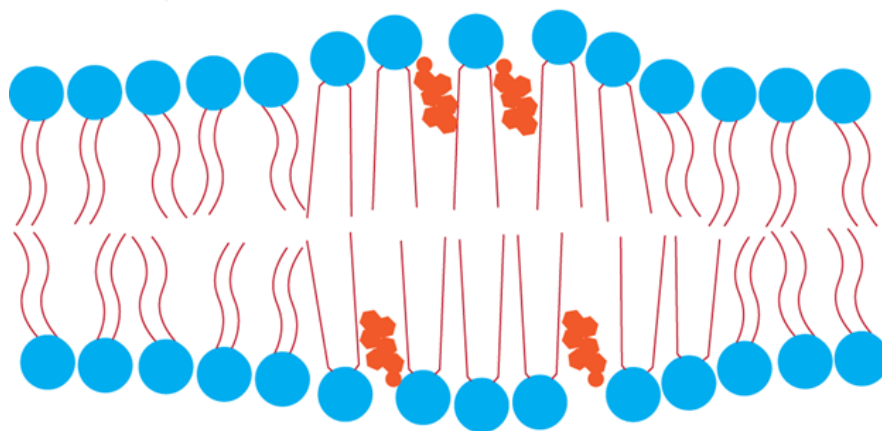
Figure 17: Cartoon model of ideal lipid bilayers composing of phospholipids (blue circle), acyl chains (red lines), and cholesterol (orange hexagons). Saturated acyl chains are more structured compared to its surrounding unsaturated acyl chains. This structural integrity stiffens L_o domains, while leaving L_d lipids to move freely around it.

3.5: T_m study of GUVs

Miscibility transition temperature T_m is the temperature where phase separated lipid

bilayers become homogeneous. To find this phase coexistence, 3:2 (DOPC:SM) + 32% Chol

GUVs were used. Given the imperfection of lipid organization, each GUV in the same batch will

not be truly homogenous in terms of the lipid content. For this fact, one can obtain small

variation of T_m in the same batch of GUV. The way T_m was extrapolated was by taking the average of two temperatures: the temperature when majority of GUVs show critical-like fluctuations (at the verge of miscibility transition temperature) and the temperature when GUVs show homogenous L_d phase. Critical-like fluctuations were found to be at 31.7°C with 32% Chol as opposed to 27°C for 35% Chol. So it seems the reduction of cholesterol resulted in temperature increase in order for GUVs to display critical-like fluctuations. Vice versa, the more cholesterol content, the smaller T_m becomes.
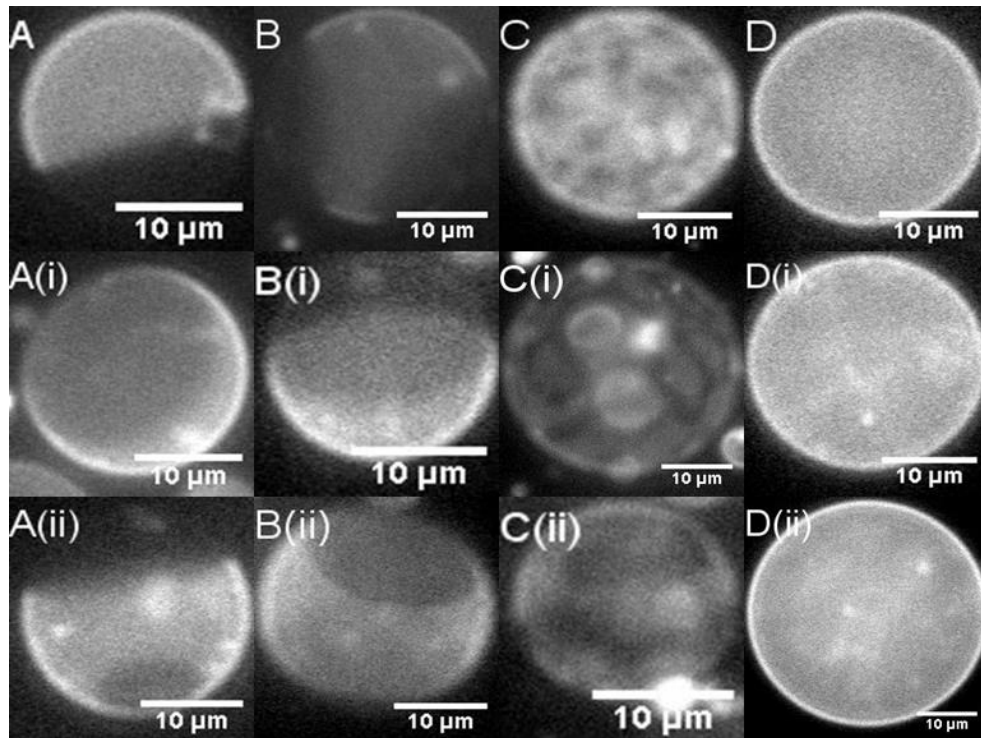
Figure 18: Above shows fluorescence GUVs temperature ramping of (3:2) DOPC:SM + 32% Chol; (A) 23.0°C; (B) 30.5°C; (C) 31.7°C-*critical fluctuations*; and (D) 35.8°C -*one L_d phase.*

As for the interaction between L_o domains and their surrounding L_d phase, the boundary is regulated by hydrophobic mismatch [25]. The L_o-L_d height difference is well established by many studies [16, 25-28]. At the boundary, L_o domain gradually decreases its height to meet with the surrounding L_d phase (smaller height) [25]. This way, the hydrophobic acyl chain of ESM on domain perimeter will not be exposed to the aqueous environment, i.e., less unfavorable energetic cost [25]. The energy per unit length at domain perimeter due to lipid bending and splaying is called line tension [29]. In other words, hydrophobic mismatch at the L_o-L_d boundaries determines line tension. Not only that, it is favorable for lipid bilayers to minimize line tension by merging multiple domains into a single giant domain over time (i.e., smallest domain perimeter when all domains are merged together). This is the reason why most GUVs display polarized domain (Figure 11). As temperature approaches T_m (from the low end), hydrophobic mismatch becomes smaller and ultimately line tension drops down to 0 at critical fluctuation regime. Figure 18 images reflect the decrease in line tension as temperature approaches T_m.

Furthermore, Veatch et al. has shown substituting brain-sphingomyelin (BSM) with egg-sphingomyelin (ESM) increases miscibility transition temperature of GUVs [18]. This means that ESM-membranes will have more stable and closely packed domains compared to those formed by BSM-membranes [17]. Also, ESM-membrane T_m allows domain formation at a wider range of temperature below T_m compared to BSM-membranes. Hence ESM was adopted instead of BSM for ternary mixture. The reason for choosing 32% cholesterol was because it falls in the liquid-

liquid coexisting region at room temperature, and the T_m at this cholesterol content is of easy

reach with our setup.

CHAPTER FOUR:

TRANSMEMBRANE DOMAIN OF THE INFLUENZA A PROTEIN

4.1: Brief introduction of M2TM

"*Flu*" is one of the oldest human companions. It is a viral infectious disease that infect, mostly, upper respiratory tract. In humans, *flu* is caused by influenza A virus. Viral envelope carrying influenza A virus enters the respiratory airway and binds to cellular membranes via viral peptide. Of course, a healthy cell does not suddenly become sick when the viral envelope gets inside host's cytoplasmic space, it is actually the release of viral code inside the viral envelope into the cytoplasmic space that infects the host cell. This viral envelope breakdown is heavily dependent on the M2 protein [30]. M2 functions to acidify viral interior to assist in envelope breakage [30]. Structurally, the transmembrane domain of M2 (M2TM) forms a tetra-oligomeric channel that allows proton transport into the viral envelope. The way protons are conducted is mediated by histidine residue (H37), which is located in the transmembrane region of M2TM [31]. Meanwhile, tryptophan residue (W41) functions as the channel gate for proton transport and is located close to the interior leaflet of viral envelope [31].

There exists enormous amount of structural studies on M2TM, but not so much on M2TM effects on critical-like fluctuations of lipid membranes. Critical-like fluctuations represent a special ability of cell membranes to modify their lipid composition at certain temperatures to

accommodate for important bioprocesses [32]. So it is significant to study how M2TM may change this innate ability of lipid membranes. M2TM peptide was incorporated into GUVs in this study. We find that inclusion of M2TM increases T_m. Not only that, smaller vesicle budding was also observed in M2TM-treated vesicles.

4.2: M2TM membrane addition approach

Two approaches were used for mixing M2TM into lipid bilayers. In the first approach, M2TM was mixed with pure lipid mixtures with desired mole ratios prior to being electroformed. The M2TM-incorporated GUVs of post-electroformation was then pipetted to silicone gel well for observation. The second approach was done by suspending M2TM in GUV buffer with 1% (v/v) DMSO. Equal volume of lipid-only GUVs and M2TM solution were pipetted into a micro-centrifuge tube (1.5 ml) and allowed to incubate for 20 minutes. After incubation, the mixture was pipetted into a silicone gel well for observation. We had also tested mixture of GUVs and DMSO as a control. For the second approach, DMSO concentration is 0.5% (v/v) and M2TM concentration is 2.3 μM.

4.3: T_m study for GUVs with M2TM

Phase miscibility transition temperature T_m for GUVs composed of (3:2) DOPC:ESM + 32% Chol was explored as a function of M2TM content. Figure 19 shows GUV miscibility transition temperature when there is 4mol%M2TM. The estimated T_m is 37 °C, which is ~5°C larger than that of GUVs without M2TM. We also performed T_m study for 1% to 8% M2TM, as shown in Figure 20 and Table 1. T_m increases steadily by 1-2 °C per 1% M2TM from 0% (32.7°C)

to 8% (48.5°C). This shows M2TM peptide indeed affects the mixing capability of lipids, i.e.,

more energy is needed to mix as M2TM % increases. Below T_m, GUVs of all M2TM % display L_o–

L_d phase separation. Phase separation becomes more prominent as the temperature drops

away from T_m.
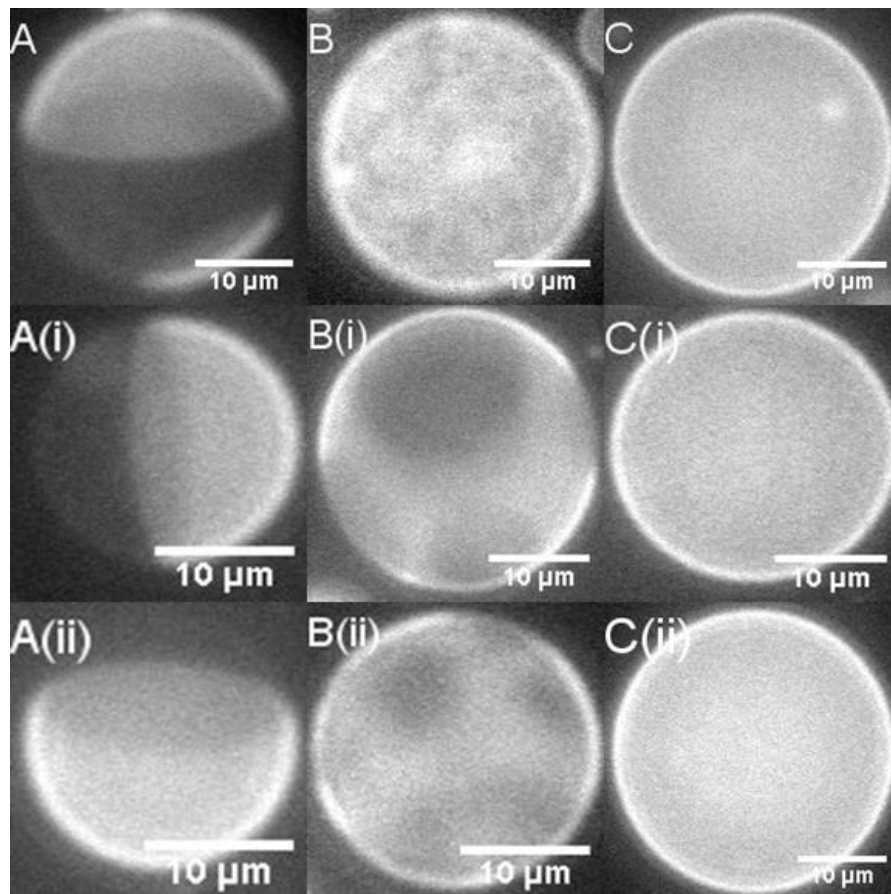
Figure 19: Above shows temperature ramping of fluorescent GUVs of (3:2) DOPC:ESM +32% Chol +4%M2TM; A) 23.0°C; (B) 37.0°C-*critical fluctuations*; and (C) >40.5°C-*one L_d phase.*
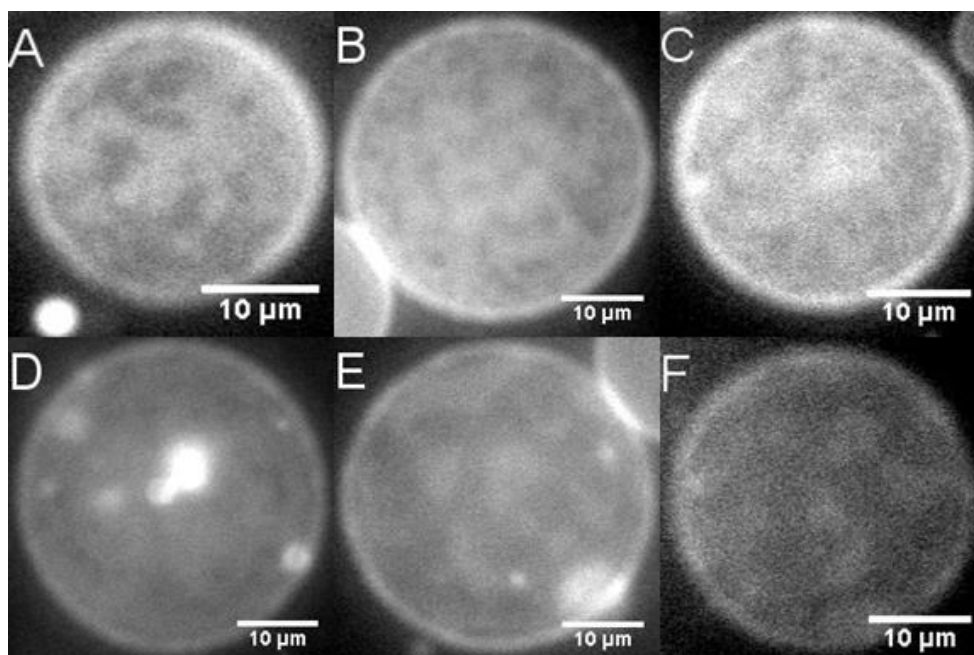
Figure 20: Above shows critical-like fluctuations of fluorescent GUVs of (3:2) DOPC:ESM +32% Chol +various %M2TM. The mole fraction of M2TM is (A) 1%(33.2°C); (B) 2%(34.5°C); (C) 4%(37.0°C); (D) 5%(39.7°C); (E) 7%(45.2°C); and (F) 8%(48.5°C).

Table 1: Summary of T_m of various M2TM % in 3:2 DOPC/ESM + 32%chol GUVs. T_m increases as M2TM % increases.

3:2 DOPC/ESM + 32%chol + M2TM %	T_m
1	33.2°C
2	34.5°C
4	37.0°C
5	39.7°C
7	45.2°C
8	48.5°C

The T_m increase in M2TM-incorporated vesicles is probably due to the partition of M2TM into L_d phase. This affinity is shown through our AFM study where we observed individual M2TM oligomers localized in the Ld phase [12]. Many factors could contribute to the phase dependent partitioning of M2TM. One possible explanation is that the length of M2TM is more compatible with the L_d phase than with the L_o phase. M2TM partitioning to the L_d region implicates a large

energy barrier between the L_o and L_d phases. This supports data of T_m increase as higher thermal energy (temperature) will be needed to cross the phase boundaries.

4.4: Vesicle budding

A group from University of Illinois has shown formation of smaller vesicles from parent GUVs, termed as "budding", with addition of pore-forming peptide is possible [33]. As has been shown by Rossman et al., M2TM is also capable of inducing vesicle budding [34]. We also studied whether M2TM can induce vesicle budding when there is Lo-Ld phase separation. The experiment was performed at 23°C for many M2TM concentrations, except for 1% M2TM. For 1% M2TM, GUV budding was observed at 33.2°C. Take 2% M2TM for example, small vesicles are observed to bud from parent GUVs with L_o and L_d phase coexistence (Figure 21). Vesicle budding persists for 4%, 5%, 7%, and 8% of M2TM (Figure 21). No budding was observed in 6% M2TM. An explanation for the lack of budding at 6% M2TM might just be due to sample preparation issue. Some parent GUVs also contain smaller vesicles inside them due to internal budding (Figure 21A-B).
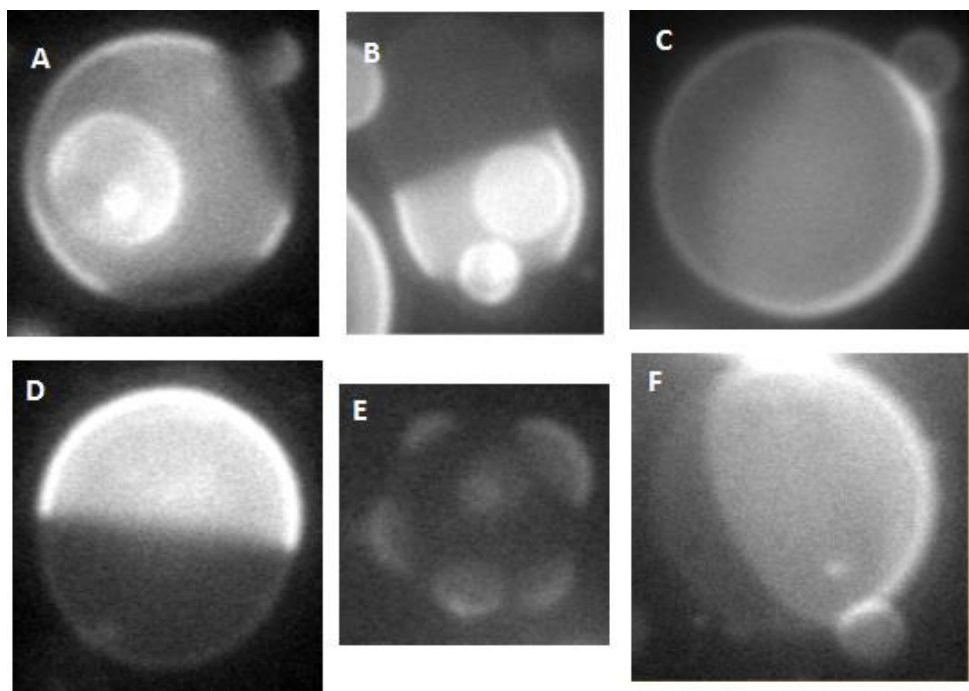
Figure 21: Above shows vesicle budding for 3:2 DOPC:ESM +32% Chol + various % M2TM at 23°C; (A) 1% (@33.2°C); (B) 2%; (C) 4%; (D) 5%; (E) 7%; and (F) 8%. For 7%, reverse budding were observed as L_d buds off vesicles instead of L_o domains.

To study if cholesterol plays a role in GUV budding, GUVs composed of 3:2 DOPC:ESM with 8% M2TM in various (2, 5,10,20) mol % cholesterol were concocted. The immediate observation is a third phase known as the gel (or solid) phase in place of the L_o phase (Figure 22). Gel phase is irregularly shaped compare to circular domains of the L_o phase. Gel phase is only present in GUVs containing 2 and 5 mol % of Chol. Budding is observed in all cholesterol mol %. Hence the amount of cholesterol plays insignificant role in GUV budding.
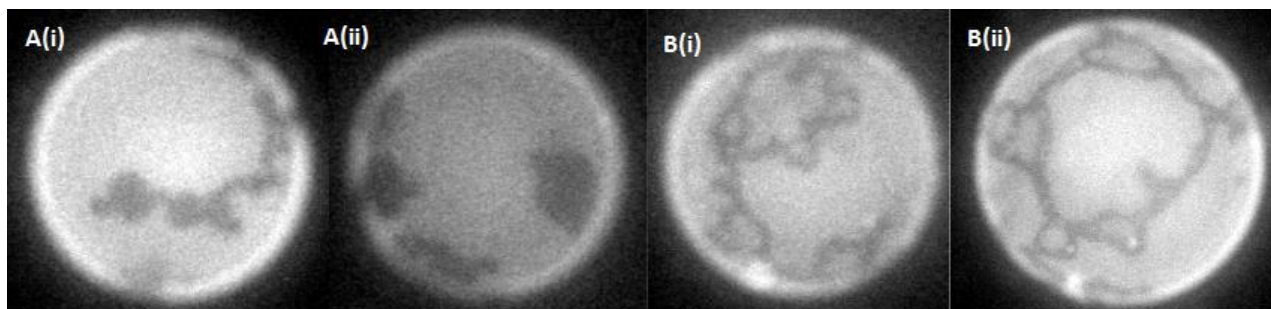
Figure 22: Above shows GUVs of 3:2 DOPC:ESM + 8% M2TM + various % Chol at 23°C. Cholesterol mole fraction is (A) 2% and (B) 5%. Low cholesterol content changed Lo domains to irregular shaped gel structure. Vesicle budding occurs at all % Chol (data are not presented).

M2TM study so far has been examined under peptide exposure with pre-electroformed lipid mixture. To test if M2TM can induce vesicle budding for lipid-only GUVs, we added M2TM dissolved in 1% DMSO to post-electroformed GUVs at 27°C. Addition of 1% DMSO only led to critical-like fluctuations at a lower temperature (27°C) of GUVs (Figure 23B). No budding is observed. Hence DMSO alone is incapable of inducing membrane budding. We noticed significantly more GUVs experiencing budding if DMSO + M2TM are added to lipid-only GUVs (Figure 23C). Also, the buddings are more distinct compared to T_m study of M2TM.
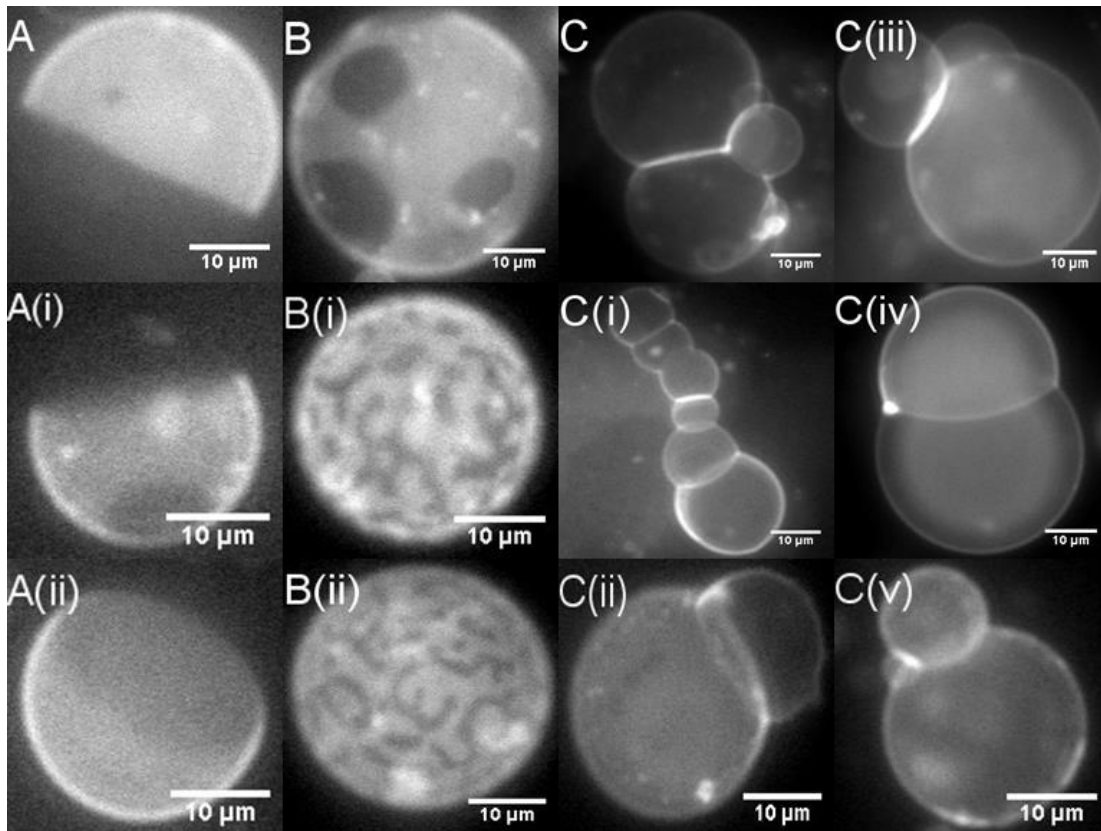
Figure 23: Above shows effect of DMSO and M2TM addition to lipid-only GUVs of (3:2) DOPC:ESM +32% Chol; (A) pure lipid; (B) 1% DMSO (27°C); and (C) 1% DMSO + 2.3 µM M2TM (budding).

M2TM has an intrinsic ability to form tetramer. This tetramer when planted into lipid membranes causes vesicle shape restructuring. The structure of tetramic M2TM is conical with tilt about 22-32° with respect to the bilayer normal [12]. The conical tetramer structure will have narrowed N-terminal and widened C-terminal. Some has reported tilt angle as large as 30-38° [35]. The tilt angle variation is believed to be caused by the length mismatch of hydrophobic thickness of different membranes and M2TM height. Within the hydrophobic region of lipid membranes, the insertion of M2TM will cause tight packing to lipid around its C-terminal compared to its N-terminal. This involuntarily shoving of lipids brings about nonsymmetrical lipid leaflet arrangement that will induce negative membrane curvature. The symmetrical

insertion of M2TM (T_m study) is why we don't see assortment of budding in M2TM-incorporated vesicles prior to electroformation. This is because the conical shape M2TM tetramer paired with symmetrical orientation will cancel out any negative curvature. On the contrary, we see a lot of budding when we introduced M2TM to lipid-only GUVs post-electroformation (Figure 23C). These budding can only mean that M2TM preferentially insert itself in one orientation more than the anti-symmetrical orientation, if added post-electroformation. One disagreement with Rossman et al. is the effect of cholesterol on vesicle budding. They reported that low cholesterol+M2 content induces budding and no budding is observed at high cholesterol+M2 content [4]. Contrary, our results tell us that cholesterol plays no role in GUV budding.

Also, our AFM data (not presented) showed that M2TM only affected lipid lateral packing and not the height of each phase. M2TM in the L_d phase increases the stiffness of that phase. The increase in L_d phase rigidity modifies line tension at domain edges. Since vesicle budding is related to domain line tension and the bending energy of budding caps, our AFM data might explain GUV budding.

CHAPTER FIVE:

POLYGLUTAMINE AGGREGATES

5.1: Brief introduction of polyglutamine

Huntingtin (htt) is the protein that is notoriously known to cause Huntington's disease (HD) in human [36-42]. The N-terminus of htt contains a stretch of glutamine amino acids (i.e., polyglutamine). The number of the consecutive glutamine amino acids was found to correlate with the onset age of HD, as well as the severity of the disease. Generally speaking, the longer the polyglutamine (polyQ) stretch is, the earlier the disease manifests itself. Moreover, when the number of glutamine is < 35, no risk of HD has been found. It seems that there is a pathologic threshold of the polyQ length [43], below which the protein is harmless and above which there is a high risk of developing the progressive neurodegenerative HD.

In HD affected patients, large aggregates of htt, the so-called inclusion bodies, have been found in various areas of dead neurons. Many biophysical and biochemical studies have shown that depending on its length, the polyQ stretch has an intrinsic tendency to aggregate into oligomers and fibrils. The similarity between polyQ aggregates and the inclusion bodies, as well as the cytotoxicity of polyQ aggregates to cultured neutrons and animal models, has led researchers to propose that polyQ is the main culprit in HD.

Despite intense research, the mechanism of polyQ mediated cellular toxicity is unknown. Several membranous targets by polyQ aggregates have been proposed, including nucleus membrane, mitochondrial inner and outer membranes, and synaptic plasma membrane. We are interested in how polyQ aggregates impair lipid membrane structure and morphology [13]. This thesis work focuses on the effect of aggregates formed by a polyQ peptide (KK-Q_{35}-KK, 35 glutamine flanked by two lysine at each end) on GUVs. GUV disruption was observed in all vesicles with addition of polyQ, as predicted. The insight of polyQ's dynamic with lipid membranes will be of significant application to therapeutic strategies.

5.2: PolyQ membrane addition approach

For polyQ study, two GUV compositions were used: pure DOPC and DOPC/ESM/Chol mixture. In both cases, polyQ aggregates were prepared by incubation in 10 mM HEPES pH 7.0 at room temperature. Aggregate formation was monitored by AFM and Fourier transform infrared spectroscopy measurements (data not shown). After confirming aggregate formation, polyQ aggregates were suspended in GUV buffer and mixed with lipid GUVs at equal volume. In other words, the polyQ solution was pipetted into GUV solution on a glass slide for imaging. Immediately after polyQ addition, fluorescence images were taken and GUVs showed no evidence of membrane disruption. For control experiment, GUV was mixed with buffer-only solution and imaged. All images of vesicle disruption obtained in this study were using 15 μM polyQ peptide and taken 10 minutes after addition.

5.3: PolyQ induces vesicle disruption

PolyQ effect on lipid membranes was first studied on single lipid GUVs made of DOPC (Figure 24A). Upon adding equal volume of 15 μM polyQ aliquot (incubated for five days at 4°C) to intact homogenous GUVs, no vesicle breakage was observed instantaneously. Peptide aliquot that was incubated for five days contains many oligomeric and fibrillar aggregates, according to our AFM data [13]. However, based on the observation that very small number of GUV breakage can be caused by directly pipetting polyQ aliquot against the GUV aliquot on a glass cover slip, we used a modified approach where GUV + polyQ aliquots were mixed in a microcentrifuge tube and let alone to incubate for 10 minutes. This approach significantly reduces artifacts associated with the pipetting procedure. Using the modified approach, we observed that GUV breakage left a residual on the glass slide that is detectable through fluorescence microscopy. The residual appears to be non-circular in shape and is generally larger in size compared to its former intact GUVs (Figure 24A:1-3).
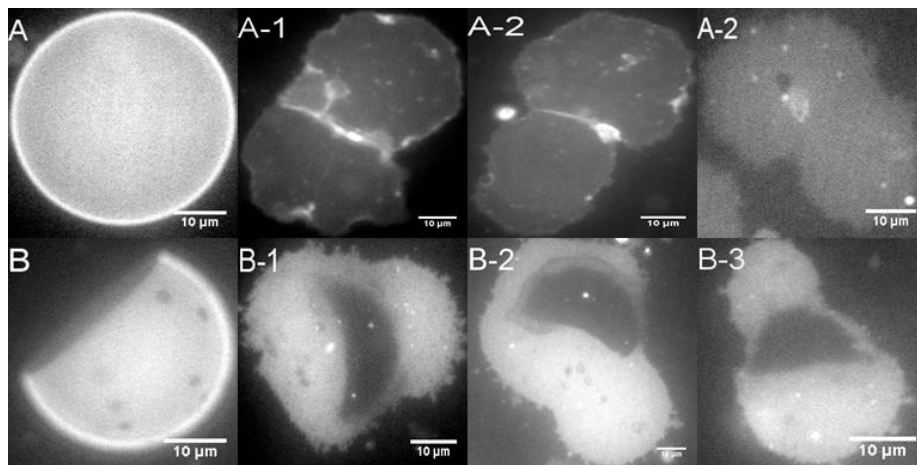
Figure 24: Above shows fluorescent GUVs vesicle breakage upon addition of polyQ (15μM) to: (A) Pure DOPC (before polyQ); A1-A3 (polyQ added) and; (B) 3:2 DOPC:ESM+20% Chol (before polyQ); B1-B3 (polyQ added). Breakage occurred about 10 minutes after polyQ aliquot added.

Ternary lipid mixture of 3:2 DOPC:ESM+20%Chol was investigated to see how polyQ affects phase-separated GUVs (Figure 24B). Similar shape and size vesicle breakage was observed 10 minutes after polyQ addition. But interestingly, the residuals from phase-separated GUVs kept their phase separation behavior even after vesicle breakage (Figure 24B:1-3).

The toxic severity of polyQ to lipid membrane draws from its own polyQ length repeat (extension) and aggregation [13, 36]. PolyQ repeats start at the N17-terminal of *htt* protein. It is headed by an N17-terminal (mainly α-helix) and is flanked by polyproline at C-terminal downstream [41, 42]. According to molecular dynamic simulations by Nagarajan et al, the combination of N17 and polyproline is key to how deep polyQ penetrates the membrane [44]. Their work also shows membrane thinning simulation data. Membrane thinning occurs in regions that contain polyQ [44]. It is safe to say then that membrane thinning can and will result in membrane disruption. Another group shares similar result with Nagarajan's group. N17-terminal of *htt* proves to be important not only to provide site for polyQ repeats, but also vital for polyQ–lipid membrane binding [45]. They presented the inhibition of N17-terminal ability to bind to lipid membrane by altering N17-terminal [45]. Kim's group reported that polyQ repeats can adopt α-helix, coil or extended loop structure [41]. They also proposed that a long (>35Q) polyQ extension will encourage the aggregation of other peptide or another extended-polyQ structure [41]. This aggregation will have pathogenic consequences on lipid membrane such as membrane disruption. Oligomer aggregate of about 6-7 monomers was reported to disrupt solid supported lipid bilayer through a two-step process, consistent with GUV result in this thesis work [42].

On a different note, the presence of cholesterol is shown to decrease polyQ binding to lipid membranes [46]. Cholesterol stiffens lipid membrane and thus reduces efficiency of polyQ to penetrate through. Contrary, our GUV data shows disrupted membrane vesicles for both pure DOPC and DOPC/ESM/Chol. This discrepancy may be due to different lipid species used and techniques employed. However, it does compel a future study of different cholesterol concentration vesicles with polyQ. One can look at the percentage of vesicle breakage and time it takes for the breakage to occur. Lastly, Chaibva et al claimed that polyQ preferentially accumulate around curved lipid membranes [47]. Chaibva finding is not covered in this work and will requires further study.

CHAPTER SIX:

POLYPHENOL DRUG MOLECULES

6.1: Brief introduction of tamoxifen, genistein, and verapamil

Of the plethora anticancer drugs used to treat breast cancer, tamoxifen, an amphiphilic molecule, has been well accepted for its use of prevention and treatment [48]. The way tamoxifen inhibit breast cancer is by competitively bind to estrogen-receptor binding sites [49]. By binding to estrogen-receptor binding sites, tamoxifen disrupts the cancer cell replication cycle. On the flip side, tamoxifen has also been shown to inhibit estrogen-receptor-negative breast cancer cells, cause liver toxicity, and antagonize protein kinase C [50-52]. Protein kinase C is key to cellular growth regulation and natural apoptotic process [53, 54]. To date, there exist numerous studies on tamoxifen-membrane interactions using fluorescence anisotropy, differential scanning calorimetry (DSC), and Fourier transform infrared (FTIR) spectroscopy. From these studies, physical and chemical properties of lipid membrane were shown to be affected by tamoxifen [55-59]. Therefore, it is deserving to know how T_m changes with tamoxifen concentration in lipid model membrane. Tamoxifen-premixed GUVs generally shows increased T_m with tamoxifen concentration, in this work.

Unlike tamoxifen, genistein and verapamil studies were ephemeral. Genistein is an isoflavones that function as estrogen receptor [60, 61]. Akin to tamoxifen, genistein can also inhibit various

cancer cell including breast cancer [62]. Aside from that, genistein is able to avert osteoporosis [63]. Verapamil is an antihypertensive drug that blocks the transport of calcium through transmembrane calcium channels [64]. It is commonly used to treat angina, arrhythmia, hypertension, and hemodynamics. Verapamil's structure is somewhat linear with a ring flanking at both ends of the carbon chain. Figure 25 shows chemical structure for tamoxifen, genistein and verapamil. On a whole, study of drug molecule affecting lipid membrane permeability is crucial because membrane poses as the first line of defense that any molecules will have to cross to get inside the cell. Though only two concentrations of genistein were studied, genistein-incorporated GUVs displays increased T_m compared to genistein-absent GUVs. As for verapamil, data shows no T_m change between verapamil-incorporated GUVs and verapamil-absent GUVs.
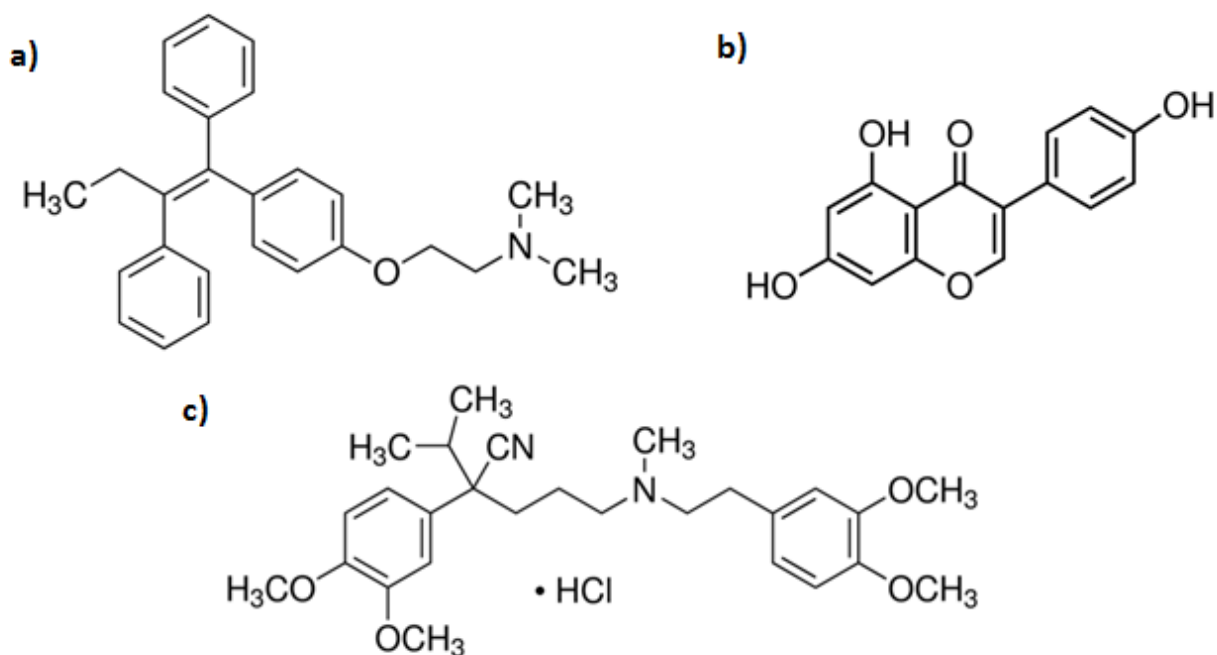
Figure 25: Chemical structure of: a) tamoxifen; b) genistein; and c) verapamil.
Image source: http://sigmaaldrich.com

6.2: T_m study of polyphenol drug molecules

      T_m study of drug molecules interacting with lipid membranes is the final work of this

thesis. Tamoxifen was added to (3:2) DOPC:ESM +32% Chol lipid mixture before GUV formation

using the electroformation method. We found that 4% tamoxifen increases GUVs T_m by about

3°C compared to lipid-only GUVs (Figure 26). Overall, as % tamoxifen increases, T_m increases by

about 1°C for 1% tamoxifen increment. A summary of T_m for 2, 4, 5, and 6% tamoxifen is shown

in Figure 27 and Table 2.
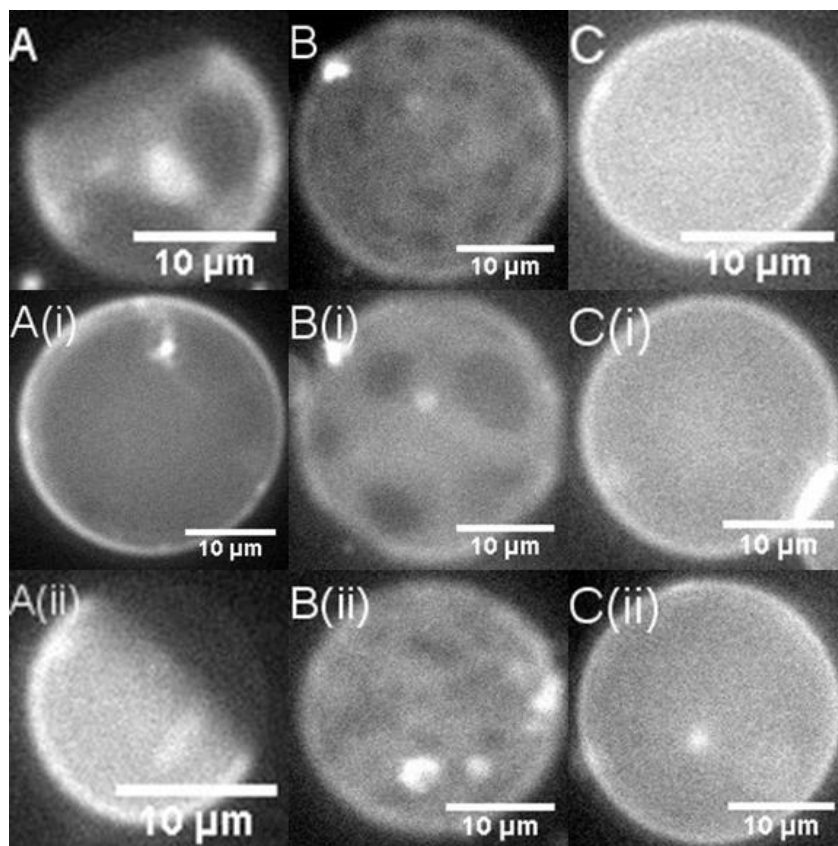
Figure 26: Above shows temperature ramping of fluorescent GUVs of (3:2) DOPC:ESM +32% Chol + 4% tamoxifen, (A) 27.0°C; (B) 36.5°C-*critical-like fluctuations*; and (C) >37.4°C-*one L_d phase.* One may note that *critical-like fluctuations* shown here resemble microdomains.
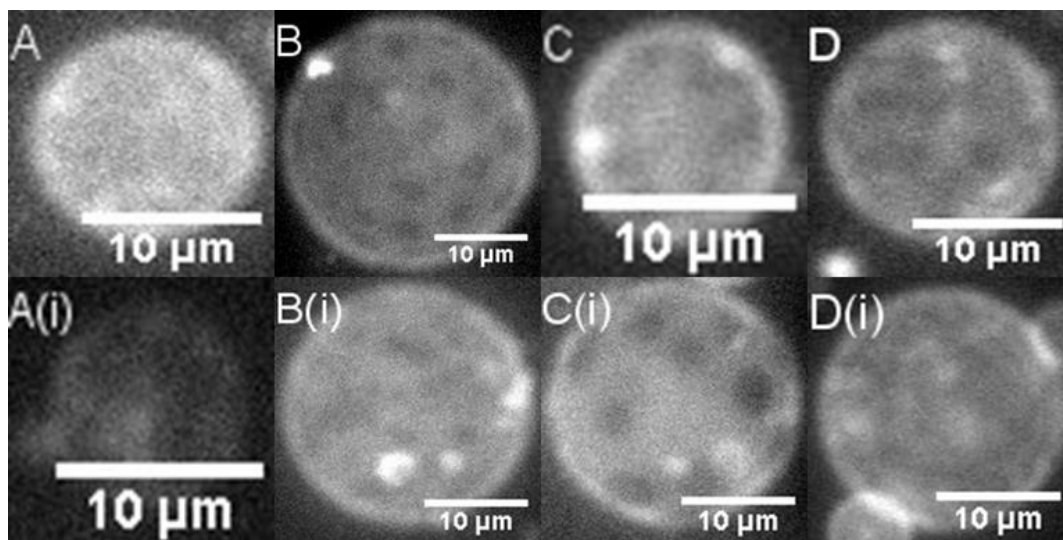
Figure 27: Above shows *critical-like fluctuations* of fluorescent GUVs of (3:2) DOPC:ESM +32% Chol + various % tamoxifen. The mole fraction of tamoxifen is (A) 2% (33.9°C); (B) 4% (36.5°C); (C) 5% (36.7°C); and (D) 6% (37.7°C). For 8% tamoxifen, due to the lack of *critical-like fluctuation* images, T_m (@37.9°C) was taken as the average of two temperatures, one from homogenous L_d phase GUVs and the other phase-separated GUVs.

Table 2: Summary of T_m of various tamoxifen % in 3:2 DOPC/ESM + 32%chol GUVs. T_m increases as tamoxifen % increases.

3:2 DOPC/ESM + 32%chol + tamoxifen %	T_m
2	33.9°C
4	36.5°C
5	36.7°C
6	37.7°C
8	37.9°C

Tamoxifen is believed to have lipid membrane rigidifying ability, similar to many flavonoids. We have reported an increased lipid membrane hydrocarbon chain thickness about 2.8 Å with tamoxifen's presence [65]. This is because tamoxifen locates itself within lipid membrane hydrophobic region [65]. Based on the observation that tamoxifen increases GUV T_m, it is likely that tamoxifen preferentially partitions into one phase versus the other (similar to M2TM).

51

Only 4 and 6% genistein were studied. Figure 28 shows critical-like fluctuations at 33.1°C for 6% genistein. Due to the lack of images with critical-like fluctuations for 4% genistein, T_m was taken as the average of two temperatures: a high temperature corresponding to homogenous L_d phase GUVs and a low temperature corresponding to phase-separated GUVs. T_m was taken to be 33.5°C for 4% genistein, which is similar to 6%. Despite an increase in T_m with genistein addition (~2°C) compared to lipid-only GUVs, result is inconclusive due to lack of studies on other genistein %.
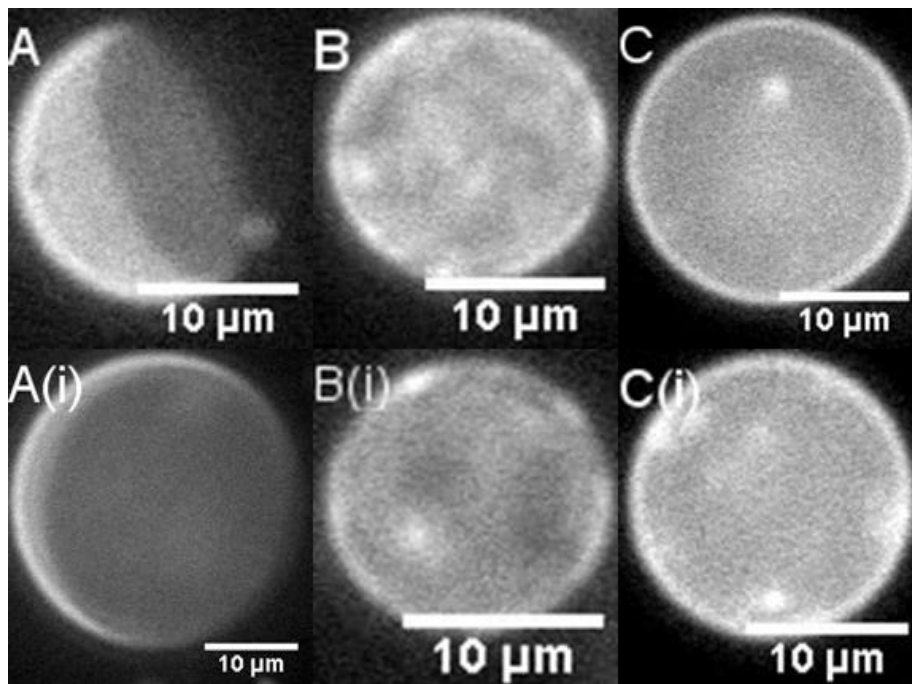
Figure 28: Above shows temperature ramping of fluorescent GUVs of (3:2) DOPC:ESM +32% Chol+6% genestein; (A) 27°C; (B) 33.1°C-*critical-like fluctuations*. and (C) >34.8°C-*one L_d phase*.

Though genistein T_m study is inconclusive, it is predicted to follow the trend of tamoxifen as genistein has similar properties to tamoxifen; genistein binds within hydrophobic region close

to the polar headgroup of lipid membranes and is capable of stiffening lipid membranes [9, 66].

Another group reported the same genistein-membrane behavior. They said genistein decreased

motional freedom of membrane polar headgroups, resulting in a more ordered membrane

structure [67]. Additionally, genistein binding is also regulated by pH of vesicles' environment

[68].

As for verapamil, 2, 4, and 8% verapamil were concocted into GUVs. Figure 29B shows critical-

like fluctuations at 31.3°C for (3:2) DOPC:ESM + 32%chol + 4% verapamil. GUVs develop into

homogenous L_d phase above 33.7°C (Figure 29C). For 2% verapamil, T_m (@31.3°C) was taken in

the same way as 4% genistein for the same reason. Similarly, 8% verapamil showed T_m at 31.4°C

(Figure 30). A summary of verapamil T_m is given in Table 3. Comparing this result with that of

lipid-only GUVs of the same lipid compositions, verapamil appears to have no effect on T_m.

Based on the augmented T_m in the presence of M2TM and tamoxifen, it is possible that

verapamil does not have a strong preference for L_o or L_d phases. Meier et al. reported that

verapamil mostly exists in a charged state at pH7.4 [69]. They also mentioned that verapamil

folds both of its aromatic ring and insert itself in the hydrophobic region of lipid membranes

while leaving the charged part of the molecule close to lipid-water interface [69]. Such a picture

may be relevant to unbiased partitioning in phase coexisting lipid bilayers.
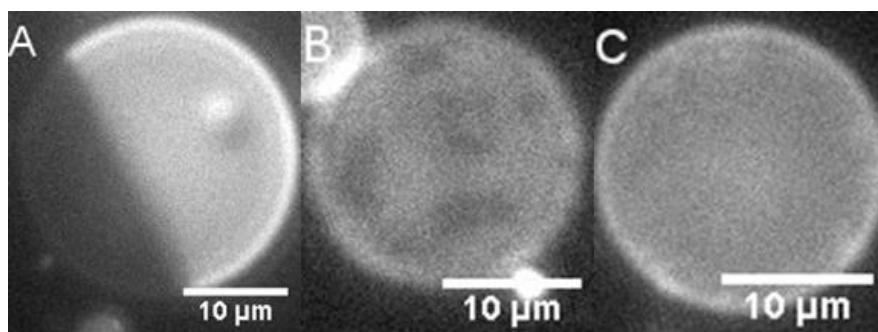
Figure 29: Above shows temperature ramping of fluorescent GUVs of (3:2) DOPC:ESM +32% Chol+4% verapamil; (A) 27°C; (B) 31.3°C-*critical-like fluctuations* and (C) >33.7°C-*one L_d phase*.
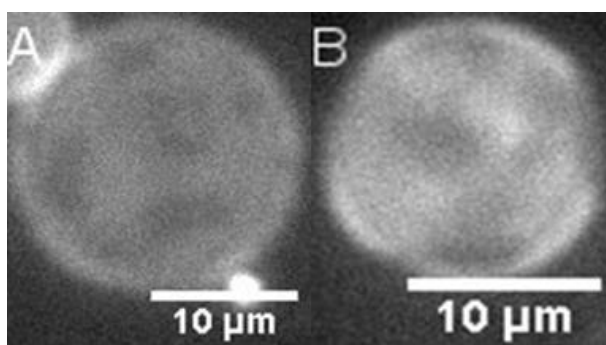
Figure 30: Above shows fluorescent GUV (3:2) DOPC:ESM+32% Chol *critical-like fluctuations* at various verapamil concentrations: (A) 4% (31.3°C) and (B) 8% (31.4°C). For 2% verapamil, due to the lack of *critical-like fluctuations* image, T_m (@31.3°C) was taken as the average of two temperatures, one from homogenous L_d phase GUVs and one from phase-separated GUVs

Table 3: Summary of T_m of various verapamil % in 3:2 DOPC/ESM + 32%chol GUVs. T_m does not change as verapamil % increases.

3:2 DOPC/ESM + 32%chol + verapamil %	T_m
2	31.3°C
4	31.3°C
8	31.4°C

CHAPTER SEVEN:

CONCLUSION

This thesis work probes various peptide/drug molecules interacting with lipid model membranes, causing T_m change, vesicle budding, and membrane disruption. With the intention to study these physical phenomena, ternary lipid model GUVs of (3:2) DOPC:ESM+32% Chol was adopted in majority parts of this thesis. The use of fluorescent microscopy and electroformation method are also vital to the study of this thesis. The main conclusions of each studies are summarized as follows:

- The increase presence of ESM and Chol in GUVs produces larger L_o domains for temperature below T_m; GUV's T_m is also modified as ESM and Chol increase.

- M2TM peptide in GUVs increase T_m; vesicle buddings is more prevalent when M2TM is added after GUVs are electroformed compared to electroformed M2TM-incorporateded GUVs; vesicle budding is caused by negative curvature induced by M2TM insertion into lipid membranes.

- Addition of polyQ (>35Q) aggregates to homogenous and phase-separated GUVs resulted in membrane rupture.

- Tamoxifen in GUVs increases T_m; genistein in GUVs increases T_m about 2°C (33.1°C) from pure ternary lipid model GUVs (T_m = 31.7°C); verapamil in GUVs has no effect on T_m.

With this, ends the journey of exploring a small piece of science on lipid membranes. The hope

of this thesis work is to provide supporting information to any research that helps in

therapeutic strategies, for the betterment of life.

BIBLIOGRAPHY

1. Hertwig, O., et al., *The cell; outlines of general anatomy and physiology*. [2d ed. 1909, London,: Sonnenschein. xvi, 368 p.

2. Fricke, H., *THE ELECTRIC CAPACITY OF SUSPENSIONS WITH SPECIAL REFERENCE TO BLOOD*. 1925. p. 137-152.

3. Gorter, E. and F. Grendel, *ON BIMOLECULAR LAYERS OF LIPOIDS ON THE CHROMOCYTES OF THE BLOOD.* The Journal of Experimental Medicine, 1925. **41**(4): p. 439-443.

4. Robertson, J.D., *The molecular structure and contact relationships of cell membranes.* Progress in biophysics and molecular biology, 1960. **10**: p. 343-418.

5. Pan, J., et al., *Using small-angle neutron scattering to detect nanoscopic lipid domains.* Chemistry and physics of lipids, 2013. **170-171**: p. 19-32.

6. Angelova, M.I., et al., *Preparation of Giant Vesicles by External Ac Electric-Fields - Kinetics and Applications.* Trends in Colloid and Interface Science Vi, 1992. **89**: p. 127-131.

7. Schmidt, N.W., et al., *Influenza Virus A M2 Protein Generates Negative Gaussian Membrane Curvature Necessary for Budding and Scission.* Journal of the American Chemical Society, 2013. **135**(37): p. 13710-13719.

8. Arribat, Y., et al., *A huntingtin peptide inhibits polyQ-huntingtin associated defects.* PloS one, 2013. **8**(7): p. e68775.

9. Engelke, M., et al., *Tamoxifen perturbs lipid bilayer order and permeability: comparison of DSC, fluorescence anisotropy, Laurdan generalized polarization and carboxyfluorescein leakage studies.* Biophysical Chemistry, 2001. **90**(2): p. 157-173.

10. Veatch, S.L., et al., *Critical fluctuations in domain-forming lipid mixtures.* Proceedings of the National Academy of Sciences of the United States of America, 2007. **104**(45): p. 17650-5.

11. Binnig, G., C.F. Quate, and C. Gerber, *Atomic force microscope.* Phys Rev Lett, 1986. **56**(9): p. 930-933.

12. Sing Ho, C., et al., *Influenza M2 Transmembrane Domain Interacting with Lipid Membranes: An Atomic Force Microscopy and Fluorescence Microscopy Study.* Biophysical Journal. **110**(3): p. 254a.

13. Ho, C.S., et al., *Polyglutamine aggregates impair lipid membrane integrity and enhance lipid membrane rigidity.* Biochim Biophys Acta, 2016. **1858**(4): p. 661-70.

14. Khadka, N.K., C.S. Ho, and J. Pan, *Macroscopic and Nanoscopic Heterogeneous Structures in a Three-Component Lipid Bilayer Mixtures Determined by Atomic Force Microscopy.* Langmuir, 2015. **31**(45): p. 12417-25.

15. Beltramo, P.J., R. Van Hooghten, and J. Vermant, *Millimeter-area, free standing, phospholipid bilayers.* Soft Matter, 2016.

16. Ho, C.S., N.K. Khadka, and J. Pan, *Sub-ten-nanometer heterogeneity of solid supported lipid membranes determined by solution atomic force microscopy.* Biochimica et biophysica acta, 2016. **1858**(2): p. 181-8.

17. London, E. and D.A. Brown, *Insolubility of lipids in triton X-100: physical origin and relationship to sphingolipid/cholesterol membrane domains (rafts).* Biochimica et biophysica acta, 2000. **1508**(1-2): p. 182-95.

18. Veatch, S.L. and S.L. Keller, *Seeing spots: complex phase behavior in simple membranes.* Biochimica et biophysica acta, 2005. **1746**(3): p. 172-85.

19. Haluska, C.K., et al., *Photo-activated phase separation in giant vesicles made from different lipid mixtures.* Biochimica et biophysica acta, 2012. **1818**(3): p. 666-72.

20. Liu, A.P. and D.A. Fletcher, *Actin polymerization serves as a membrane domain switch in model lipid bilayers.* Biophysical journal, 2006. **91**(11): p. 4064-70.

21. Gandhavadi, M., et al., *Structure, composition, and peptide binding properties of detergent soluble bilayers and detergent resistant rafts.* Biophysical journal, 2002. **82**(3): p. 1469-82.

22. Patra, S.K., et al., *Liposomes containing sphingomyelin and cholesterol: Detergent solubilisation and infrared spectroscopic studies.* Journal of Liposome Research, 1999. **9**(2): p. 247-260.

23. Lonnfors, M., et al., *Sterols Have Higher Affinity for Sphingomyelin than for Phosphatidylcholine Bilayers even at Equal Acyl-Chain Order.* Biophysical Journal, 2011. **100**(11): p. 2633-2641.

24. Portet, T., S.E. Gordon, and S.L. Keller, *Increasing Membrane Tension Decreases Miscibility Temperatures; an Experimental Demonstration via Micropipette Aspiration.* Biophysical Journal, 2012. **103**(8): p. L35-L37.

25.   Kuzmin, P.I., et al., *Line tension and interaction energies of membrane rafts calculated from lipid splay and tilt.* Biophysical journal, 2005. **88**(2): p. 1120-33.

26.   Bleecker, J.V., et al., *Thickness Mismatch of Coexisting Liquid Phases in Noncanonical Lipid Bilayers.* The journal of physical chemistry B, 2016. **120**(10): p. 2761-70.

27.   Morein, S., et al., *The effect of peptide/lipid hydrophobic mismatch on the phase behavior of model membranes mimicking the lipid composition in Escherichia coli membranes.* Biophysical journal, 2000. **78**(5): p. 2475-85.

28.   Wallace, E.J., N.M. Hooper, and P.D. Olmsted, *Effect of hydrophobic mismatch on phase behavior of lipid membranes.* Biophysical journal, 2006. **90**(11): p. 4104-18.

29.   Garcia-Saez, A.J., S. Chiantia, and P. Schwille, *Effect of line tension on the lateral organization of lipid membranes.* The Journal of biological chemistry, 2007. **282**(46): p. 33537-44.

30.   Gu, R.X., L.A. Liu, and D.Q. Wei, *Drug Inhibition and Proton Conduction Mechanisms of the Influenza A M2 Proton Channel.* Advance in Structural Bioinformatics, 2015. **827**: p. 205-226.

31.   Wang, C., R.A. Lamb, and L.H. Pinto, *Activation of the M2 ion channel of influenza virus: a role for the transmembrane domain histidine residue.* Biophys J, 1995. **69**(4): p. 1363-71.

32.   Connell, S.D., et al., *Critical point fluctuations in supported lipid membranes.* Faraday Discussions, 2013. **161**: p. 91-111.

33.   Yu, Y., et al., *Vesicle Budding Induced by a Pore-Forming Peptide.* Journal of the American Chemical Society, 2010. **132**(1): p. 195-201.

34. Rossman, J.S., et al., *Influenza Virus M2 Protein Mediates ESCRT-Independent Membrane Scission.* Cell, 2010. **142**(6): p. 902-913.

35. Gu, R.-X., et al., *Free energy calculations on the two drug binding sites in the M2 proton channel.* Journal of the American Chemical Society, 2011. **133**(28): p. 10817-25.

36. *A novel gene containing a trinucleotide repeat that is expanded and unstable on Huntington's disease chromosomes. The Huntington's Disease Collaborative Research Group.* Cell, 1993. **72**(6): p. 971-83.

37. Ravina, B., et al., *The relationship between CAG repeat length and clinical progression in Huntington's disease.* Movement disorders : official journal of the Movement Disorder Society, 2008. **23**(9): p. 1223-7.

38. DiFiglia, M., et al., *Aggregation of huntingtin in neuronal intranuclear inclusions and dystrophic neurites in brain.* Science (New York, N Y), 1997. **277**(5334): p. 1990-3.

39. Penney, J.B., Jr., et al., *CAG repeat number governs the development rate of pathology in Huntington's disease.* Annals of neurology, 1997. **41**(5): p. 689-92.

40. Snell, R.G., et al., *Relationship between trinucleotide repeat expansion and phenotypic variation in Huntington's disease.* Nature genetics, 1993. **4**(4): p. 393-7.

41. Kim, M.W., et al., *Secondary structure of Huntingtin amino-terminal region.* Structure (London, England : 1993), 2009. **17**(9): p. 1205-12.

42. Caron, N.S., et al., *Polyglutamine domain flexibility mediates the proximity between flanking sequences in huntingtin.* Proceedings of the National Academy of Sciences of the United States of America, 2013. **110**(36): p. 14610-5.

43.   Zoghbi, H.Y. and H.T. Orr, *Glutamine repeats and neurodegeneration.* Annu Rev

        Neurosci, 2000. **23**: p. 217-47.

44.   Nagarajan, A., S. Jawahery, and S. Matysiak, *The Effects of Flanking Sequences in the*

        Interaction of Polyglutamine Peptides with a Membrane Bilayer. The Journal of Physical

        Chemistry B, 2014. **118**(24): p. 6368-6379.

45.   Burke, K.A., et al., *Huntingtin disrupts lipid bilayers in a polyQ-length dependent manner.*

        Biochimica Et Biophysica Acta-Biomembranes, 2013. **1828**(8): p. 1953-1961.

46.   Gao, X., et al., *Cholesterol Modifies Huntingtin Binding to, Disruption of, and*

        Aggregation on Lipid Membranes. Biochemistry, 2016. **55**(1): p. 92-102.

47.   Chaibva, M., K.A. Burke, and J. Legleiter, *Curvature enhances binding and aggregation of*

        huntingtin at lipid membranes. Biochemistry, 2014. **53**(14): p. 2355-65.

48.   Clarke, M., et al., *Tamoxifen for early breast cancer: An overview of the randomised*

        trials. Lancet, 1998. **351**(9114): p. 1451-1467.

49.   Shiau, A.K., et al., *The structural basis of estrogen receptor/coactivator recognition and*

        the antagonism of this interaction by tamoxifen. Cell, 1998. **95**(7): p. 927-37.

50.   Yang, L.H., et al., *Survival benefit of tamoxifen in estrogen receptor-negative and*

        progesterone receptor-positive low grade breast cancer patients. J Breast Cancer, 2012.

        15(3): p. 288-95.

51.   O'Brian, C.A., et al., *Inhibition of protein kinase C by tamoxifen.* Cancer Res, 1985. **45**(6):

        p. 2462-5.

52.   Ribeiro, M.P., A.E. Santos, and J.B. Custodio, *Mitochondria: the gateway for tamoxifen-*

        induced liver injury. Toxicology, 2014. **323**: p. 10-8.

53.   Eyster, K.M. and M.R. Clark, *Nonsteroidal antiestrogen inhibition of protein kinase C in human corpus luteum and placenta.* Biochem Pharmacol, 1989. **38**(20): p. 3497-503.

54.   Hayon, T., et al., *Non-steroidal antiestrogens induce apoptosis in HL60 and MOLT3 leukemic cells; involvement of reactive oxygen radicals and protein kinase C.* Anticancer Res, 1999. **19**(3A): p. 2089-93.

55.   Custodio, J.B., L.M. Almeida, and V.M. Madeira, *The anticancer drug tamoxifen induces changes in the physical properties of model and native membranes.* Biochim Biophys Acta, 1993. **1150**(2): p. 123-9.

56.   Wiseman, H., P. Quinn, and B. Halliwell, *Tamoxifen and related compounds decrease membrane fluidity in liposomes. Mechanism for the antioxidant action of tamoxifen and relevance to its anticancer and cardioprotective actions?* FEBS Lett, 1993. **330**(1): p. 53-6.

57.   Wiseman, H. and P. Quinn, *The Antioxidant Action of Synthetic Estrogens Involves Decreased Membrane Fluidity - Relevance to Their Potential Use as Anticancer and Cardioprotective Agents Compared to Tamoxifen.* Free Radical Research, 1994. **21**(3): p. 187-194.

58.   Suwalsky, M., et al., *Interaction of the anticancer drug tamoxifen with the human erythrocyte membrane and molecular models.* Zeitschrift Fur Naturforschung C-a Journal of Biosciences, 1998. **53**(3-4): p. 182-190.

59.   Boyar, H. and F. Severcan, *Tamoxifen-model membrane interactions: An FT-IR study.* Journal of Molecular Structure, 1997. **408**: p. 265-268.

60.   Pawlikowska-Pawlega, B., et al., *Localization and interaction of genistein with model membranes formed with dipalmitoylphosphatidylcholine (DPPC).* Biochim Biophys Acta, 2012. **1818**(7): p. 1785-93.

61.   Nehybova, T., et al., *Wedelolactone induces growth of breast cancer cells by stimulation of estrogen receptor signalling.* Journal of Steroid Biochemistry and Molecular Biology, 2015. **152**: p. 76-83.

62.   Gupta, S., F. Afaq, and H. Mukhtar, *Involvement of nuclear factor-kappa B, Bax and Bcl-2 in induction of cell cycle arrest and apoptosis by apigenin in human prostate carcinoma cells.* Oncogene, 2002. **21**(23): p. 3727-3738.

63.   Szkudelska, K. and L. Nogowski, *Genistein - A dietary compound inducing hormonal and metabolic changes.* Journal of Steroid Biochemistry and Molecular Biology, 2007. **105**(1-5): p. 37-45.

64.   Erdreich, A. and H. Rahamimoff, *The inhibition of Ca uptake in cardiac membrane vesicles by verapamil.* Biochem Pharmacol, 1984. **33**(14): p. 2315-23.

65.   Khadka, N.K., et al., *Interactions of the anticancer drug tamoxifen with lipid membranes.* Biophysical journal, 2015. **108**(10): p. 2492-501.

66.   Raghunathan, M., et al., *Structure and Elasticity of Lipid Membranes with Genistein and Daidzein Bioflavinoids Using X-ray Scattering and MD Simulations.* Journal of Physical Chemistry B, 2012. **116**(13): p. 3918-3927.

67.   Pawlikowska-Pawlega, B., et al., *Biophysical characterization of genistein-membrane interaction and its correlation with biological effect on cells - The case of EYPC liposomes and human erythrocyte membranes.* Biochimica Et Biophysica Acta-Biomembranes, 2014. **1838**(8): p. 2127-2138.

68.   Ollila, F., et al., *Characterization of flavonoid--biomembrane interactions.* Archives of biochemistry and biophysics, 2002. **399**(1): p. 103-8.

69.   Meier, M., et al., *Interaction of verapamil with lipid membranes and P-glycoprotein: Connecting thermodynamics and membrane structure with functional activity.* Biophysical Journal, 2006. **91**(8): p. 2943-2955.

Electroformation Procedure

Materials: 200mM Sucrose solution, 200mM Glucose solution, 0.48 mg/ml DPPE-rhodamine in chloroform, 2mg/ml DOPC in chloroform, 2mg/ml ESM in chloroform, 2mg/ml Chol in chloroform, propanol, ITO (Indium Tin Oxide) slides, O-rings, paper clips, conductor-coated alligator clips wire, syringes, vacuum pump, pastuer pipet, VWR heating system with aluminum block

Preparation:

1) Clean ITO slides and O-ring with propanol. After dried, wipe ITO slides (both sides) and Pastuer pipette with lens paper. Set aside.

2) Clean syringes with chloroform. Set aside.

3) Warm up sucrose, glucose, dye, lipid to room temperature. Set aside.

4) Heat and stabilize cleaned ITO slides, O-ring, Pasteur pipette, and aluminum block to about 55°C. We use hot plate.

Method:

1) Syringe 50μl of 2mg/ml DOPC, 30μl of 2mg/ml ESM, 19μl of 2mg/ml Chol, 2μl of 0.48mg/ml DPPE-rhodamine, and 99μl of chloroform into a glass test tube.

2) Vortex solution by Fisher fixed speed vortex mixer for 1 minute.

3) Syringe 50µl of mixed solution onto conductive side and top part of an ITO slide.
   REMEMBER: ITO slides should be about 55°C (refer Preparation step 4).

4) Gently roll solution over the top half on ITO slide until a thin layer of lipid was
   formed using the curved body of Pasteur pipette. Another 50µl of mixed solution
   syringe onto the same spot on the same ITO slide. "Roll" action performed to get a
   thin layer of lipid.

5) Repeat Method step 3 and 4 for other ITO slides. 4 slides corresponded to 2 samples
   in aluminum block.

6) Vacuum ITO slides for about 45-60 minutes using vacuum pump.

7) Heat ITO slides back to about 55°C.

8) Place O-ring on top of the lipid film formed on the ITO slide. Place another ITO slide
   with film layer touching the O-ring, like a sandwich. Press the "O-ring-ITO sandwich"
   firmly without causing O-ring to move to ensure O-ring sticks to one of the ITO
   slides. Slowly peel off one ITO slide, O-ring will stick to one of the ITO slide.

9) Once O-ring joined with one ITO slide, place identical O-ring at the bottom half of
   the joined ITO slide. Then pipet 500µl of 0.2M Sucrose into the O-ring with lipid film,
   and immediately but carefully cover with another ITO slide like the sandwich in
   Method step 8.

10) Clip the "sandwich" at the bottom half of ITO slides-O-ring sandwich using paper
    clip.

11) Soak the leakage away with Kim wipes if there are leakage.

12) Slide the sandwich into one of the slot in the aluminum block.

13) Hook alligator clip wires from a function generator to the slides.

14) Set function generator parameter to use sine wave, 2Vpp and 10Hz.These

parameters can be changed to experiment on the size of GUVs. Apply voltage for 2

hours under these setting when aluminum block hits 60°C. Shut off function

generator after 2 hours. Allow aluminum block to cool down gradually from 60 to

22°C over the span of 10 hours. Temperature is controlled by Digi-Sense

temperature controller.

Harvesting:

1) Remove alligator clips from ITO slides and unclip the O-ring-ITO sandwich.

2) Carefully pry open one side of ITO slide and then pipet out the GUV solution in the

O-ring into 2ml of 200mM Glucose. Gently homogenize the GUV solution in glucose.

3) Clean ITO slides and O-rings with propanol and store in pure water.

APPENDIX B

Programming Digi-Sense Temperature Controller

To program Digi-Sense temperature controller:

i)   Turn power on, and you will see 2 rows of number. The red number represent current temperature the probe is reading. The yellow number below it represent set/desired temperature.

ii)   To change desired temperature to a different value, simply press the "up arrow" or "down arrow" button. The "infinity" button acts like an exit button. The "green" button brings you to the menu. I never use the "EZ" button.

iii)   Press and hold "green" button for 3 seconds and you will see the screen below:

There are 4 programmable programs, denoted by P1 through P4. To see them, use "up/down arrow". NOTE: P1 is already programmed for GUV synthesis from 60-22 °C. So select P2 or others to start programming.

iv)   To select P2, press the "green" button. The scree will display

Number 11 is basically step 1 for profile 2. This number 11 will go up to

20, which allow 10 steps for programming. If you choose P3, you will see

21 which corresponding to step 1 of profile 3.

v)   At number 11, press "green" button once. You will see

t_1 represent time. You can press "up/down arrow" to look at other type

of heating mode. At t_1 screen, press "green" button. This allows you to

set your desired temperature and duration of heating.

You set by using "up/down arrow" then confirm it by pressing the "green" button once.

vi)   After this, the screen below will appear

Make sure Ent 1 and 2 are both "off". Use "up/down arrow".

You will then be directed to this page again. Up to this point, you have successfully program temperature and duration of heating in step 1.

vii)   Press "infinity" button to exit previous screen and go back to

Now use 12 to program step 2.

Repeat procedure (v) to (vii) for subsequent steps. Once you have

programmed   all the steps, press "infinity" button few times until you get

to the home screen   with 2 numbers

To start the programmed program:

i)   Turn power on.

ii)   Press "green" button until you see screen below. You might see 11 instead of 1,

        use "up/down arrow" to adjust.

This is step 1 in profile 1. To get to step 1 in profile 2, use "up/down arrow"

button to go   to 11.

Then press "green" button to get to the screen below

Use "up/down arrow" button to change the screen to "step" as below

Then click the "green" button. This runs the program. And you will see this

screen

The number below changes because it is ramping up to set value. The

"mountain" icon to the right of the bottom number shows that the program is

running.

iii)   To end the profile, press "green" button until you see screen below

, if you are running profile 1

, if you are running profile 2

Press "green" button and you will see screen below

Use "up/down arrow" button to get to "End" like screen below

Press "green" button and this will end the temperature ramping.

APPENDIX C

Publications

- Chian Sing Ho, Nawal K. Khadka, Fengyu She, Jianfeng Cai, and Jianjun Pan*. Influenza M2 Transmembrane Domain Senses Membrane Heterogeneity and Enhances Membrane Curvature. Langmuir **2016**, DOI: 10.1021/acs.langmuir.6b00150.

- Chian Sing Ho, Nawal K. Khadka, Fengyu She, Jianfeng Cai, and Jianjun Pan*. Polyglutamine Aggregates Impair Lipid Membrane Integrity and Enhance Lipid Membrane Rigidity. Biochimica et Biophysica Acta - Biomembranes **2016**, 1858: 661-670.

- Chian Sing Ho, Nawal K. Khadka, and Jianjun Pan*. Sub-Ten-Nanometer Heterogeneity of Solid Supported Lipid Membranes Determined by Solution Atomic Force Microscopy. Biochimica et Biophysica Acta - Biomembranes **2016**, 1858: 181-188.

- Nawal K. Khadka, Chian Sing Ho, and Jianjun Pan*. Macroscopic and Nanoscopic Heterogeneous Structures in a Three-Component Lipid Bilayer Mixtures Determined by Atomic Force Microscopy. Langmuir **2015**, 31: 12417-12425.

- Nawal K. Khadka, Xiaolin Cheng, Chian Sing Ho, John Katsaras, and Jianjun Pan*. Interactions of the Anticancer Drug Tamoxifen with Lipid Membranes. Biophysical Journal **2015**, 108: 2492-2501.

- Jianjun Pan, Xiaolin Cheng, Melissa Sharp, Chian Sing Ho, Nawal Khadka, John Katsaras. Structural and Mechanical Properties of Cardiolipin Lipid Bilayers Determined Using

Neutron Spin Echo, Small Angle Neutron and X-ray Scattering, and Molecular Dynamics

Simulations. Soft Matter **2014**, 11:130-138.